PNL-6887
UC-25

4B

# Freeze-Dried Processing of Tungsten Heavy Alloys

G. D. White
W. E. Gurwell

June 1989

Prepared for the U.S. Department of Energy
under Contract DE-AC06-76RLO 1830

Pacific Northwest Laboratory
Operated for the U.S. Department of Energy
by Battelle Memorial Institute

Battelle

PNL-6887

## DISCLAIMER



PACIFIC NORTHWEST LABORATORY
*operated by*
BATTELLE MEMORIAL INSTITUTE
*for the*
UNITED STATES DEPARTMENT OF ENERGY
*under Contract DE-AC06-76RLO 1830*

Printed in the United States of America
Available from
National Technical Information Service
United States Department of Commerce
5285 Port Royal Road
Springfield, Virginia 22161

NTIS Price Codes
Microfiche A01

Printed Copy

| Pages | Price Codes |
|---|---|
| 001-025 | A02 |
| 026-050 | A03 |
| 051-075 | A04 |
| 076-100 | A05 |
| 101-125 | A06 |
| 126-150 | A07 |
| 151-175 | A08 |
| 176-200 | A09 |
| 201-225 | A10 |
| 226-250 | A11 |
| 251-275 | A12 |
| 276-300 | A13 |

PNL-6887
UC-25

# FREEZE-DRIED PROCESSING OF TUNGSTEN HEAVY ALLOYS

G. D. White
W. E. Gurwell

June 1989

Prepared for
the U.S. Department of Energy
under Contract DE-AC06-76RLO 1830

Pacific Northwest Laboratory
Richland, Washington 99352

## SUMMARY

Tungsten heavy alloy powders were produced from freeze-dried aqueous solutions of ammonium metatungstate and, principally, sulfates of Ni and Fe. The freeze-dried salts were calcined and hydrogen reduced to form very fine, homogenous, low-density, W heavy alloy powders having a coral-like structure with elements of approximately 0.1 $\mu$m in diameter. The powders yield high green strength and sinterability. Tungsten heavy alloy powders of 70%, 90%, and 97% W were prepared by freeze drying, compacted, and solid-state (SS) sintered to full density at temperatures as low as 1200°C and also at conventional liquid-phase (LP) sintering temperatures.

Solid-state sintered microstructures contained polygonal W grains with high contiguity; the matrix did not coat and separate the W grains to form low-contiguity, high-ductility structures. Liquid-phase sintered microstructures were very conventional in appearance, having W spheroids of low contiguity. All these materials were found to be brittle. High levels of residual S accompanied by segregation of the S to all the microstructural interfaces are principally responsible for the brittleness; problems with S could be eliminated by using Fe and Ni nitrates rather than the sulfates.

Unusually high hardness, approaching 48 HRC, was obtained from sintering at 1130°C. As-sintered hardness decreases as grain size increases with sintering temperature during SS sintering and with time during LP sintering. The relationship between grain size and hardness follows the Hall-Petch relationship. Theoretically, as-sintered hardnesses approaching 60 HRC are possible at sintering temperatures circa 1000°C if hot isostatic pressing or some other mechanical process is employed to achieve full densification.

## ACKNOWLEDGMENTS

This work was sponsored by the United States Army Ballistic Research Laboratory and the Army Material Technology Laboratory. Valuable contributions to this work were made by the following Pacific Northwest Laboratory (PNL) staff: L. A. Charlot, N. C. Davis, J. L. Humason, R. H. Jones, and C. B. Ruhter. T. W. Penrice of Teledyne Firth Sterling generously provided valuable technical insights. K. A. Parnell edited this report.

CONTENTS

## FIGURES

TABLES

# INTRODUCTION

The cryochemical or freeze-dry process is a method for preparing both oxide and metal powders with excellent properties, that are extremely fine and homogenous with high green strength and sinterability. Landsberg and Campbell reported and patented the process for preparing tungsten (W) and tungsten-rhenium (W-Re) powders by freeze drying (Landsberg and Campbell 1965; Landsberg 1967). Since their work was published, other investigators have used the process to prepare and characterize other metal, oxide, and carbide powders (Roehrig and Wright 1972). An excellent description and technical discussion of the process is included in the article by Schnettler, Monforte, and Rhodes (1968).

In the work reported here, the freeze-dry process was employed to prepare W heavy alloys, W-Ni-Fe. This approach was judged to be promising with respect to alloy properties because of the homogeneity, small particle size, and improved sinterability demonstrated in other systems. Sintered specimens with extremely uniform and fine-textured microstructures have been produced from these powders.

The objective of this investigation was the production of an improved, higher-strength W heavy alloy through finer microstructures obtainable from powders prepared by the freeze-dry process.

## CONCLUSIONS AND RECOMMENDATIONS

Freeze-dried W heavy alloy powders are fine and homogenous and have high green strength and sinterability, full densification being attained at 1200°C. Solid-state (SS) sintered microstructures contained polygonal W grains with apparently high contiguity; the matrix did not coat and separate the W grains to form low-contiguity, high-ductility structures, as hoped. However, the ductility-structure relationship was not demonstrated in this work due to the embrittling effects of residual S and, perhaps, other elements. Additional work needs to be done using S-free solutions, and with careful attention to other potentially embrittling elements such as O; only then will the possibilities for high strength and toughness be determined.

Liquid-phase (LP) sintered microstructures were similar to those obtained from conventional powders. Less than 10-min LP sintering produces somewhat finer structures that should have higher strength. Such "flash" sintering requires precise control of heat flow and temperature, conditions which may be attainable only in very small parts. Therefore, flash LP sintering should be of secondary interest in any future work.

As-sintered hardnesses increase as grain size decreases with lowered sintering temperature. The relationship between hardness and grain size follows the Hall-Petch relationship and as-sintered hardnesses near 48 HRC were attained. Even higher hardnesses, approaching 60 HRC, are theoretically possible through mechanically augmented sintering processes, such as hot isostatic pressing. Therefore, unique combinations of high hardness, density, and conductivity are possible from freeze-dried W heavy alloys. Applications should be considered for these materials that would benefit from these properties (for example, small caliber projectiles, wear parts, and electrical contacts).

## POWDER PREPARATION

Through the freezing and drying operation, the preparation of powders is similar to the commercial freeze-dry processing of foods or beverages. A solution is flash frozen and dried; but, in addition, the anhydrous salts produced in freeze drying must be converted to the desired end product by thermal treatments. The process consists of the following operations:

- preparing a solution containing the metal salts that will decompose to the desired metal composition
- flash freezing the solution by spraying it into a very cold liquid that is immiscible with the solution
- drying the frozen solution in vacuum at a temperature below the freezing temperature of the solution
- decomposing the salt to form the oxides
- reducing the oxides to metal alloy.

The final product is extremely friable aggregates composed of crystallites less than 1000 Å in size. The low bulk density of the powder requires it to be prepressed and granulated before compacting for sintering. Powder compacts have high green strength and sinterability. Fine, homogenous, sintered microstructures are obtained.

## SOLUTION PREPARATION

Solutions for this work were prepared using ammonium metatungstate (AMT) and either the sulfates or nitrates of Ni and Fe. Initial attempts were made to synthesize the alloy powder using tungstic acid or ammonium paratungstate, but it was difficult to prepare clear, stable solutions. The AMT is very soluble in water and was found to be very convenient for laboratory use. Its large solubility (>1000 g/L) allowed solution concentrations of 100 to 200 g metal alloy per L; in fact, the limiting solubilities were the sulfates in the higher Ni-Fe composition.

In preparing the solutions, the AMT and Ni-Fe salts were dissolved separately in distilled water and the two combined before dilution to the desired

concentration. These solutions were stable and could be stored up to 48 h without becoming turbid or precipitating the salts. However, solutions prepared for this work were frozen within 1 h after preparation.

Solutions containing the Ni-Fe nitrates had to be neutralized with the ammonium ion (using ammonium hydroxide) before freezing. Otherwise, the salts would not precipitate during the freezing operation and the frozen solution cannot be dried.

Three alloy compositions were prepared for this work: 97W-2.1Ni-0.9Fe, 90W-7Ni-3Fe, and 70W-21Ni-9Fe.

## FLASH FREEZING

Flash freezing was accomplished by spraying the salt solutions through a 0.02-in.-diameter orifice into rapidly stirred hexane which was maintained at temperatures between -70°C and -50°C during the freezing operation.

The hexane was contained in a large stainless steel beaker fitted with a basket sieve. After freezing, the frozen product, in the form of microspheres, was removed from the hexane in the basket sieve, allowed to drain, and transferred to precooled trays in a freezer. Freezer storage of 24 h or more allowed residual hexane to evaporate before drying commenced.

## DRYING

Drying takes place by vacuum sublimation of the frozen water from the frozen microspheres. The drying was done in a lab-size freeze dryer with shelf temperature control, product (microsphere) temperature measurement capability, condenser temperature capability of -80°C, and a vacuum pumping rate of 190 L/min.

Shelf temperature was set initially at -25°C for receiving the trays of frozen product. After a vacuum of less than 200-$\mu$m Hg was obtained, the shelf temperature was reset at -2°C. The product temperature remained at or slightly below -25°C until the ice sublimation was essentially complete, at which time the temperature of the microsphere would rise to near the shelf temperature set point. Simultaneously, the vacuum would improve to less than

50-$\mu$m Hg. At this time the shelf temperature was reset at 40°C. When the product temperature reached 40°C, the product (Figure 1) was removed from the dryer.

## DECOMPOSITION AND CALCINING

Thermogravimetric analysis in air of the as-dried product indicated that decomposition was complete at 750°C as no further weight loss occurred above this temperature. Therefore, decomposition and calcining was done at 750°C to 850°C for 2 h in air flows of 15 cfh through 1-$ft^3$ furnace volume for 100 to 800 g of metal content. Figure 2 is an example of a decomposed and calcined product.

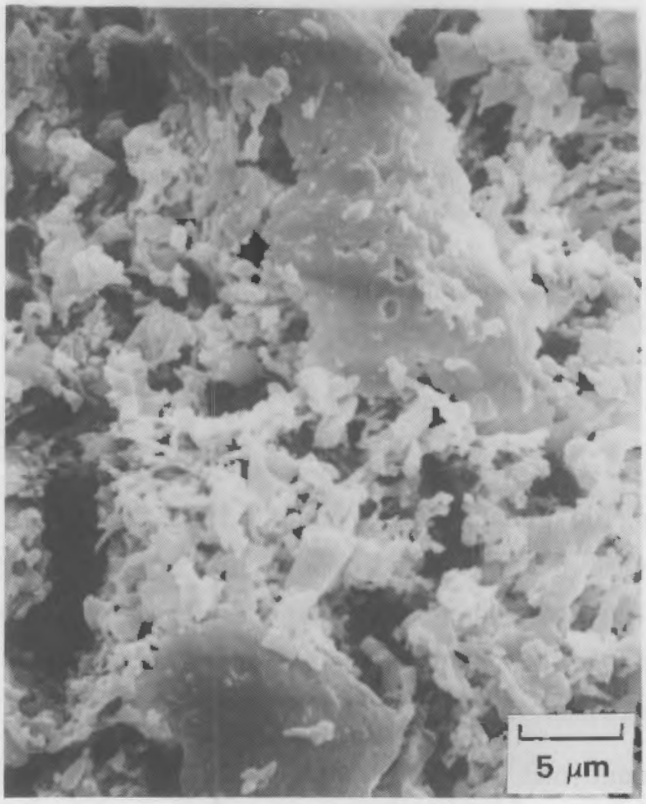


FIGURE 1. Scanning Electron Micrograph of Dried Microsphere Surface. From solution of AMT and Ni-Fe sulfates for production of 90W-7Ni-3Fe alloy.

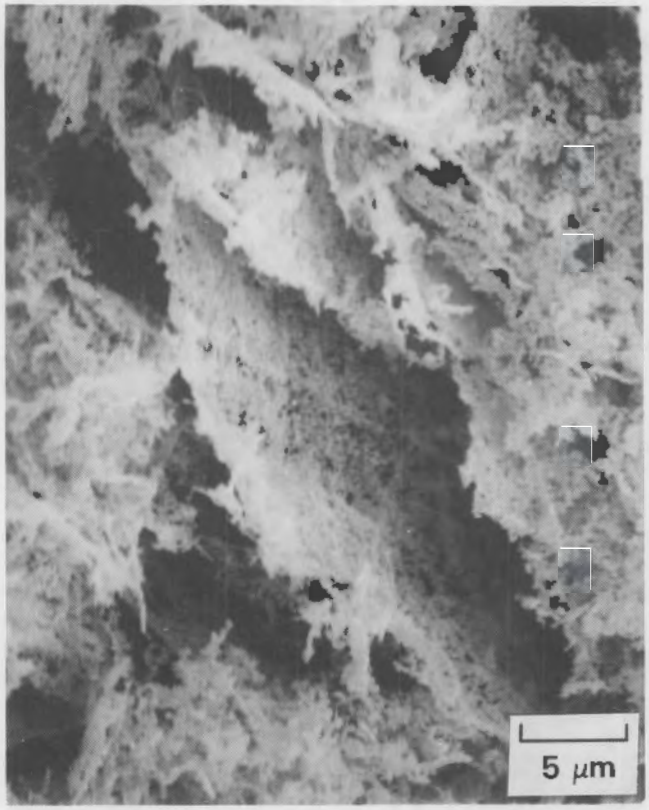


FIGURE 2. Scanning Electron Micrograph of Decomposed and Calcined Granule Surface from AMT and Ni-Fe Sulfate Salts to Produce 90% W Alloy Composition

## REDUCTION

The calcined oxide product was reduced in a cold-wall furnace with W mesh heating elements in 100% $H_2$. Temperatures of reduction were between 825°C and 950°C. The reduced powder (Figure 3) was black with low bulk density. The powder could be compacted without any binder or lubricant, producing strong specimens.

Some early reductions were run in $H_2$ 20% Ar. Evidently, in this atmosphere, reduction was not complete since specimens made from this powder blistered during LP sintering.

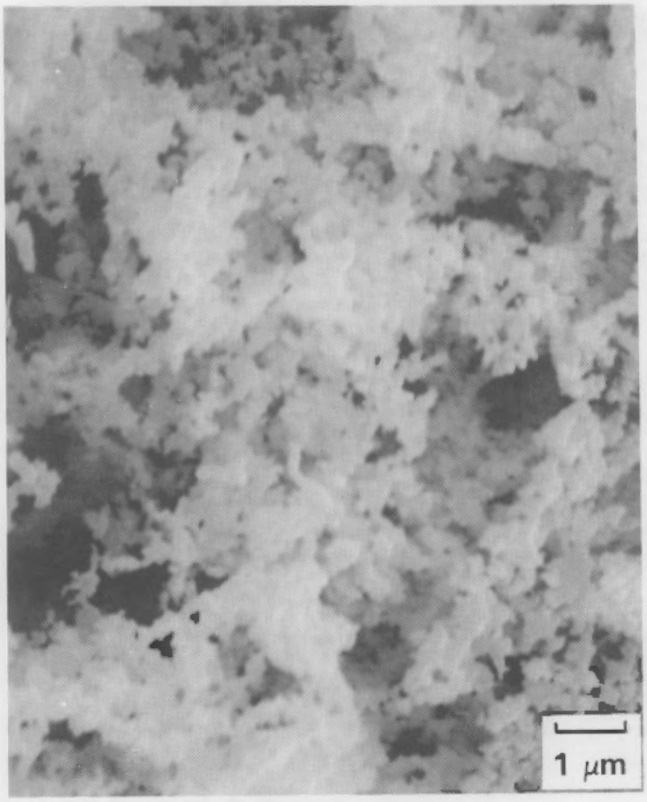


FIGURE 3. Scanning Electron Micrograph of 90W-7Ni-3Fe Alloy Powder Granule Surface

## POWDER COMPACTION

Because of low bulk density, the as-reduced powders were generally precompacted at 6 Kpsi and granulated to 20 mesh to produce a denser press feed. Buttons pressed at 25 Kpsi in a 0.45-in.-diameter die were shiny, sharp edged, and strong.

## SINTERABILITY

An investigation was done to show the effect of reduction temperature on sinterability. Two solutions of compositions were prepared to produce 90W-7Ni-3Fe. The AMT was the W source for both compositions, but the Ni and Fe were introduced either as sulfates or as nitrates. Both solutions were processed as previously described. The decomposition-calcining temperature was 750°C for both powders and the reduction temperatures were 836°C, 867°C, and 930°C for each. Buttons were pressed at 25 Kpsi after the powders had been precompacted at 6 Kpsi and granulated to 20 mesh.

The alloy buttons were sintered in a cold-walled furnace with W mesh elements and in a flowing 100% $H_2$ atmosphere. The heating ramp included a 1 h hold at 880°C. The cooling ramp included a 1 h hold at 1000°C after changing the atmosphere to 100% Ar. Sintering temperatures were 1030°C, 1130°C, and 1240°C with a 2 h hold at each temperature.

The sinterability results (density versus sintering temperature) for each powder and reduction temperature are plotted in Figure 4. These results indicate that sinterability of the powders decreases with increasing reduction temperature between 836°C and 930°C, and the sulfate-derived powders are more sinterable than those derived from nitrate. However, buttons from all reductions approach full density when sintered at 1240°C.

Microstructures of buttons sintered at 1240°C are shown in Figures 5 and 6. No strong differences are apparent between the structures. Grain sizes of the W phase are primarily in the 2- to 5-$\mu$m range and grain shape varies from euhedral to anhedral. Although all microstructures exhibit high contiguity of W grains, the nitrate-derived alloy structures show intergrowth of the W grains much more than is evident with the sulfate-derived alloy.

A second test was done to determine the effect of decomposition-calcining temperature on sinterability. Alloy composition was again 90W-7Ni-3Fe and the Ni-Fe components were derived from sulfates. Processing was the same as previously described except calcining temperatures were 800°C and 850°C, each held for 2 h. Both powders were reduced at 880°C in 100% $H_2$.

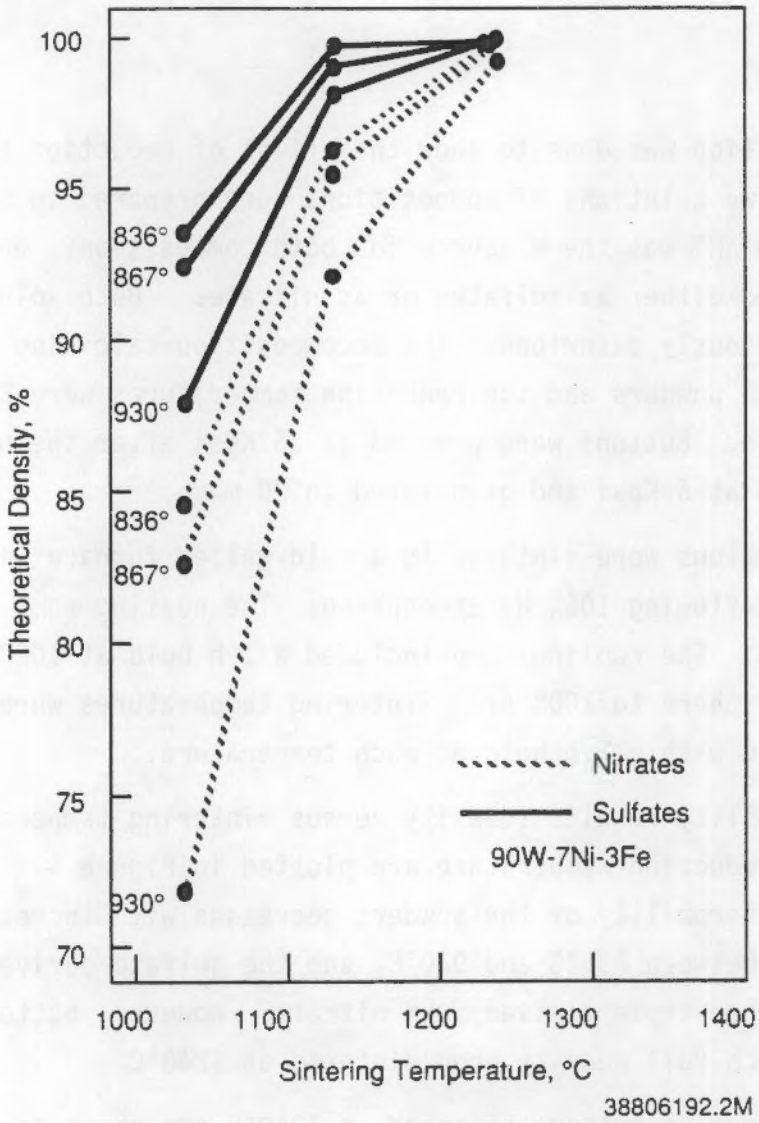


FIGURE 4. Sinterability Versus Reduction Temperatures for Alloy Powders Derived from AMT and Either Nitrates or Sulfates of Ni and Fe (sintering time of 2 h)

Figure 7 is a plot of density versus sintering temperature for buttons from each of the calcine temperatures. Although sinterability does decrease with rising calcination temperature, the effect is less pronounced than that of reduction temperature.

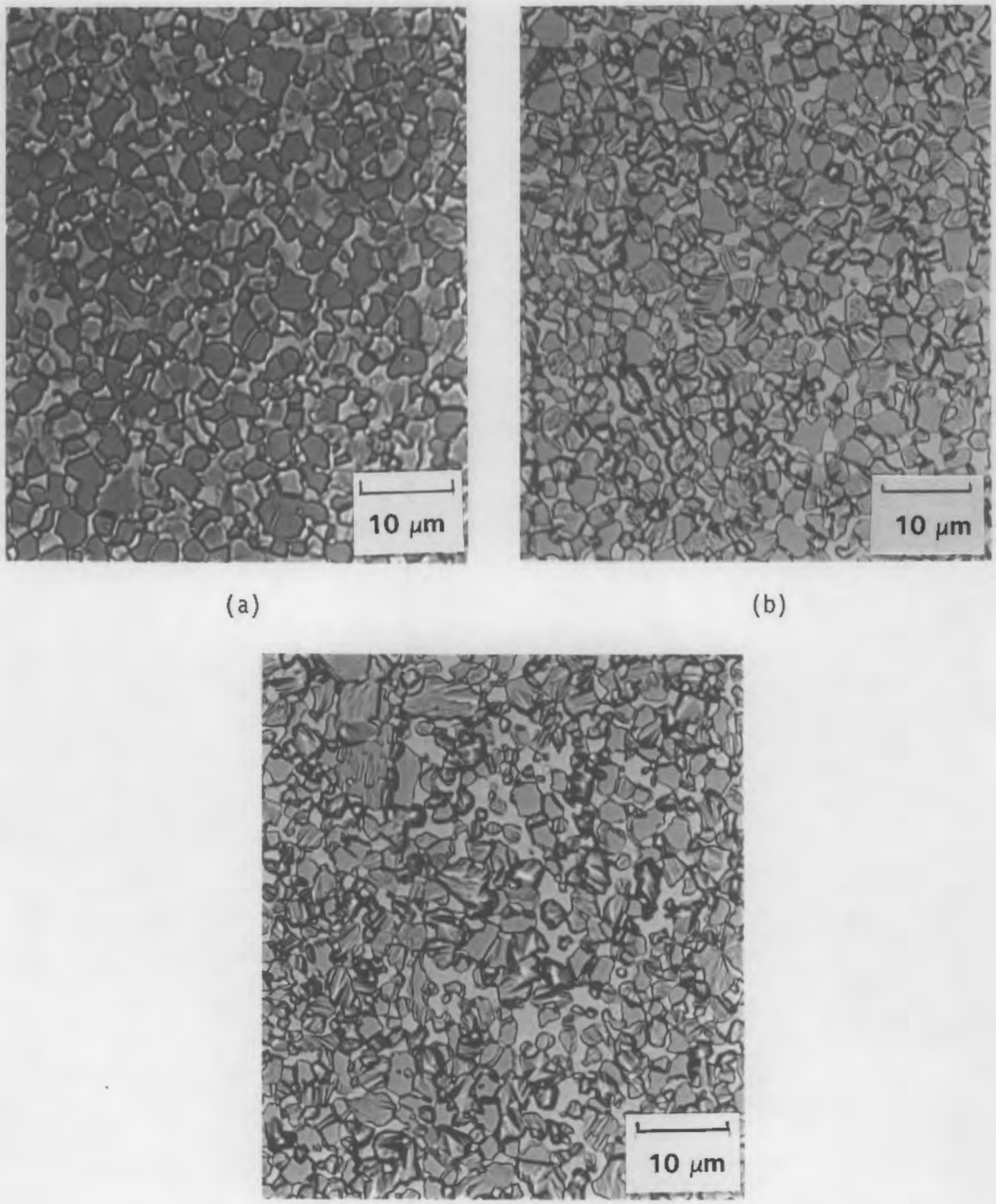


(a) (b)

(c)

FIGURE 5. Metallographs of Sulfate-Derived 90W-7Ni-3Fe Alloy Buttons Sintered for 2 h at 1240°C in $H_2$. Reduction temperatures were (a) 836°C, (b) 867°C, and (c) 930°C.

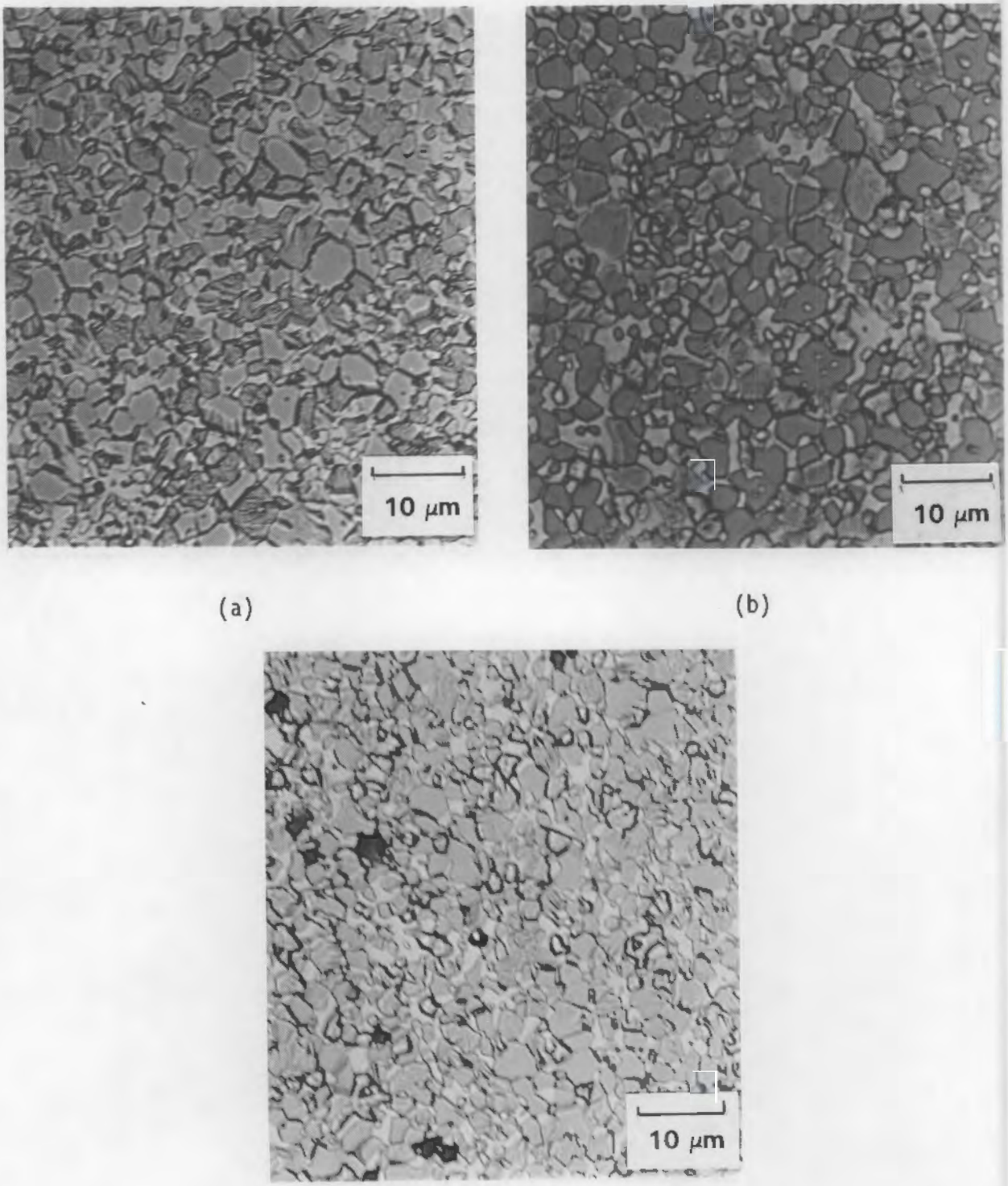


(a) (b)

(c)

FIGURE 6. Metallographs of Nitrate-Derived 90W-7Ni-3Fe Alloy Buttons Sintered for 2 h at 1240°C in $H_2$. Reduction temperatures were (a) 836°C, (b) 867°C, and (c) 930°C.

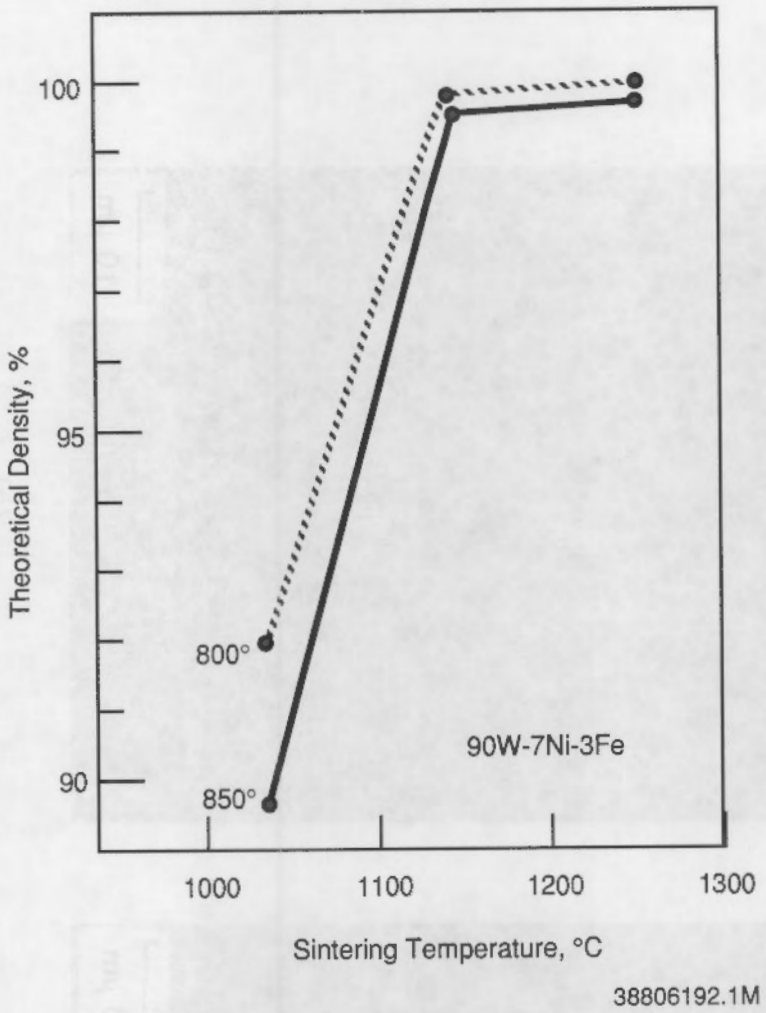


FIGURE 7. Sinterability Versus Calcination Temperatures for Alloy Powders Derived from AMT and Sulfates Reduced at 880°C (calcining for 2 h)

Microstructures of sintered buttons from each of the calcining temperatures are shown in Figure 8. The structures are similar in both grain size and grain morphology. Tungsten grain contiguity is evident in both structures.

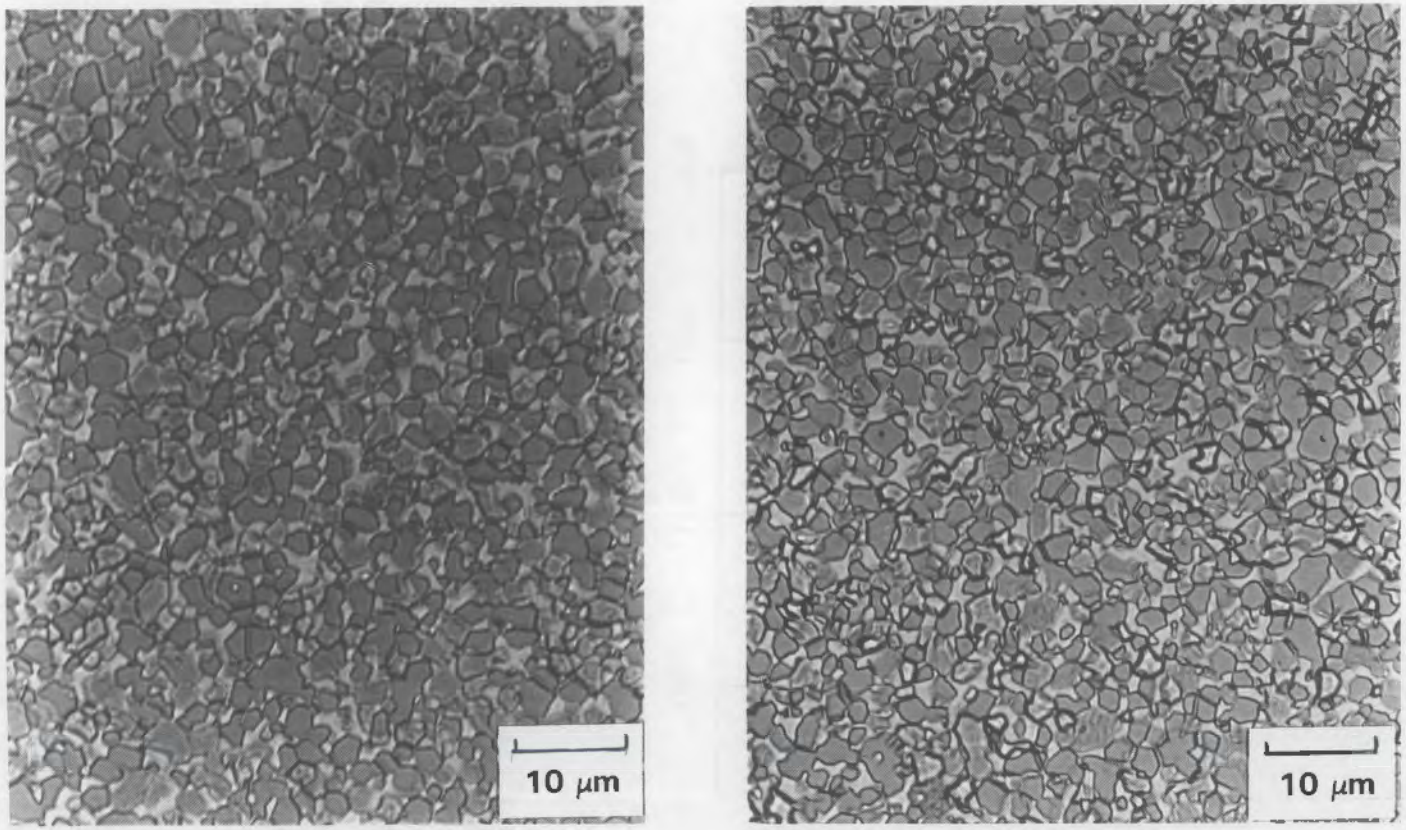


(a) (b)

FIGURE 8. Metallographs of 90W-7Ni-3Fe Alloy Buttons Sintered at 1240°C for 2 h in $H_2$. Sulfate-derived powders were decomposed and calcined at (a) 800°C and (b) 850°C for 2 h in air flows of 15 cfh. Reduced at 880°C.

## LIQUID-PHASE SINTERING

Two additional compositions were prepared for the LP sintering work, 97W-2.1Ni-0.9Fe and 70W-21Ni-9Fe. They were processed in the same manner as described previously with a decomposition-calcining temperature of 800°C for 2 h in air and reduction in 100% $H_2$ at 880°C for 2 h. Buttons were pressed from the powders after recompaction and granulation, as done previously.

The buttons were ramped at 700°C/h in 100% $H_2$ with a 1 h hold at 880°C. At 1400°C, the $H_2$ atmosphere was replaced with 100% Ar before soaking for 4, 8, and 16 min at a furnace control temperature of 1495°C. The temperature at the buttons was near 1475°C. Cooling in Ar was at 1000°C/h with a 1 h hold at 1000°C. During sintering, the buttons rested on alumina tile and were shielded from direct radiation from the heating elements.

As can be seen in the micrographs of Figures 9, 10, and 11, showing the microstructures of 70%, 90%, and 97% W compositions, respectively, the buttons heated for 4 min did not develop an LP. The W grains still have the blocky and irregular shapes of SS sintering. However, when held at temperature for 8 min, the structures indicate the presence of an LP as evidenced by the presence of rounded W grains with some grains not yet showing the effect of the liquid. Except for the 97% W composition, specimens held for 16 min at temperature show the complete transformation of the W phase by liquid to rounded grains. The transformation of the 97% W composition appears to be incomplete. Figure 10 has an additional micrograph of the 90% W composition LP sintered for 40 min; the microstructure shown is identical to that obtained from conventional powders, which are typically LP sintered 30 to 40 min. After transforming from the SS to the LP sintered structure, the W grains exhibit much less contiguity. For the structures held for 16 min at temperature, the W grain sizes increase with W content: 10 to 16 $\mu$m for the 70% W composition, 14 to 22 $\mu$m for the 90% W composition, and 16 to 24 $\mu$m for the 97% W composition. From these results, it appears that each of these compositions would require a discrete time and temperature combination for optimum LP sintering results.

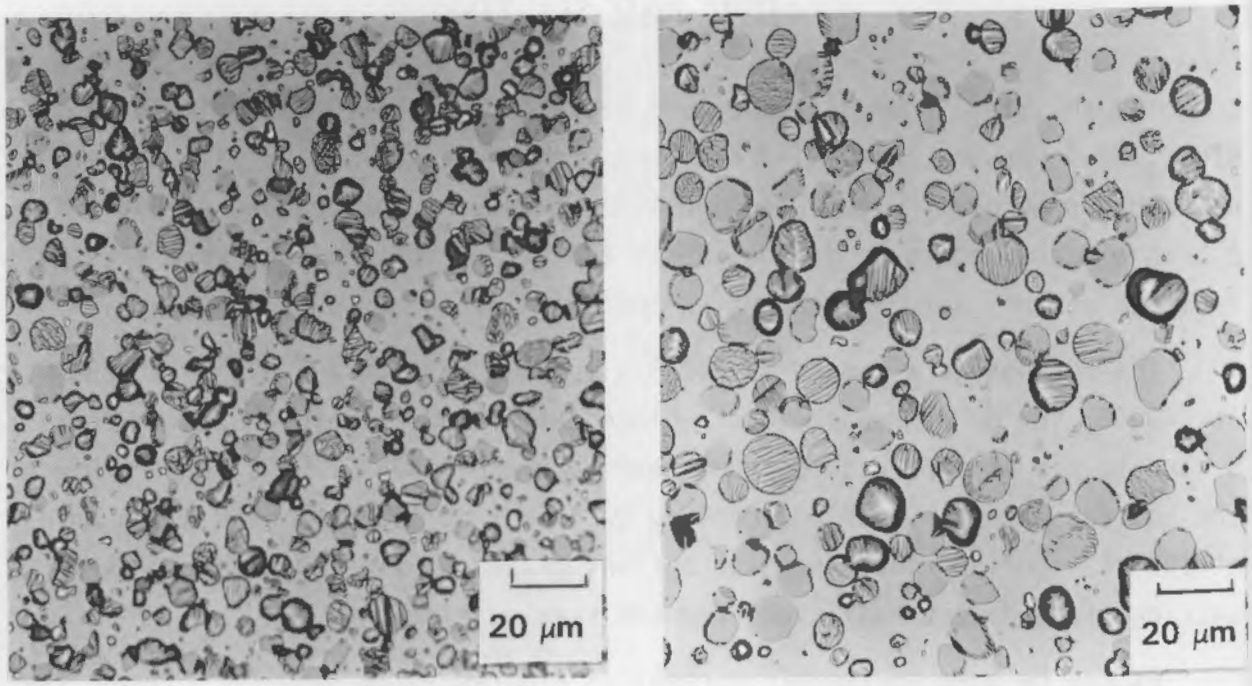


(a) (b)

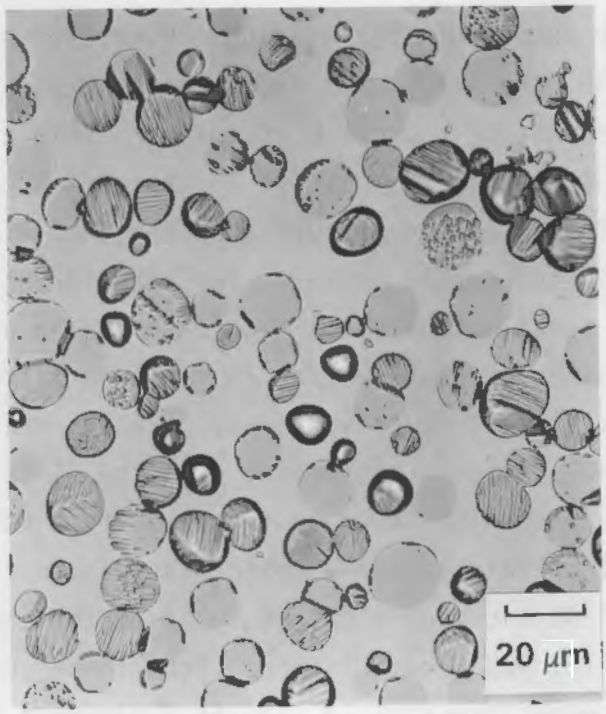


(c)

FIGURE 9. Metallographs of 70W-21Ni-9Fe Alloy Buttons Sintered at 1495°C (furnace control temperature) for (a) 4, (b) 8, and (c) 16 min

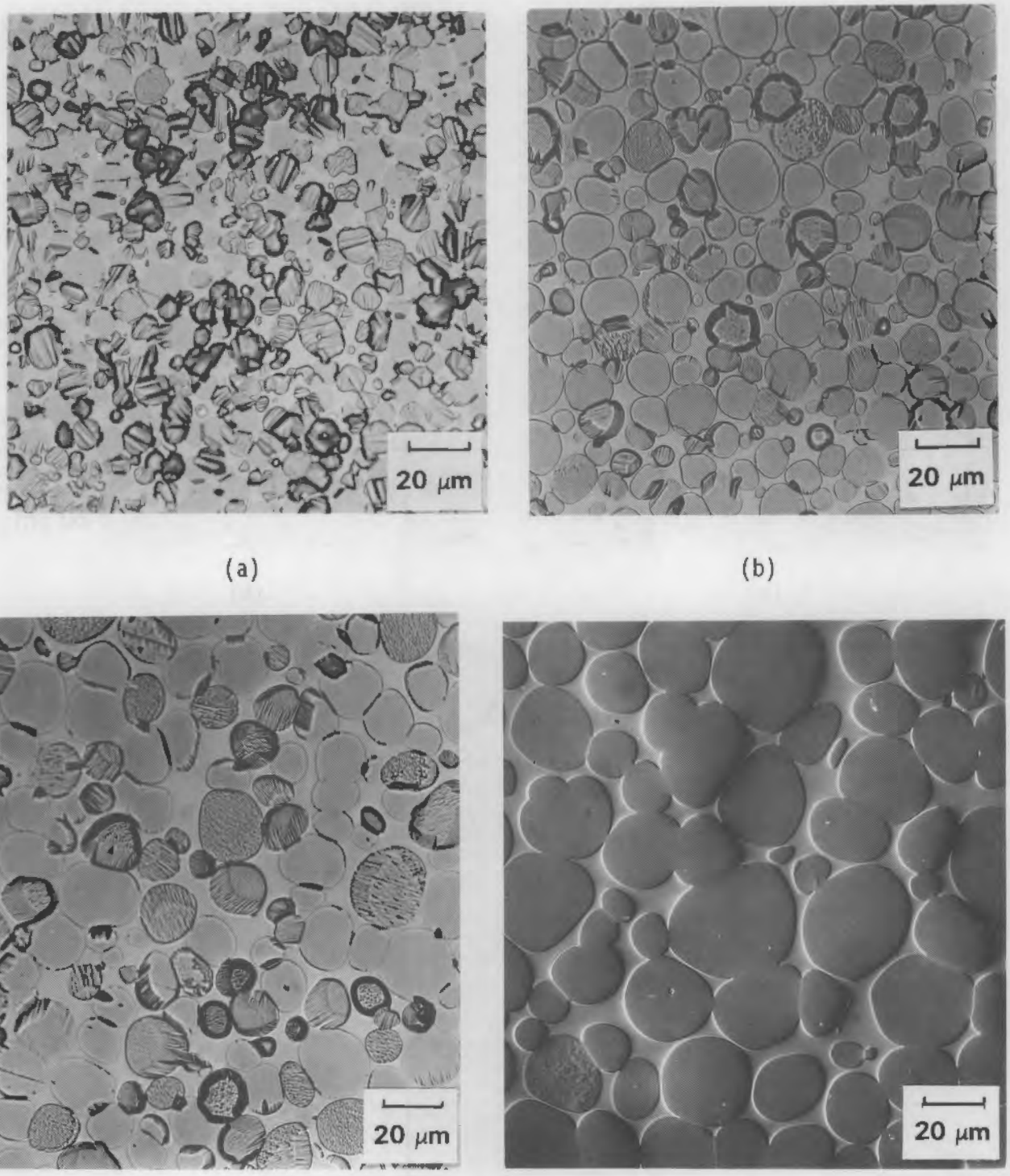


(a) (b)

(c) (d)

FIGURE 10. Metallographs of 90W-7Ni-3Fe Alloy Buttons Sintered at 1495°C (furnace control temperature) for (a) 4, (b) 8, (c) 16, and (d) 40 min

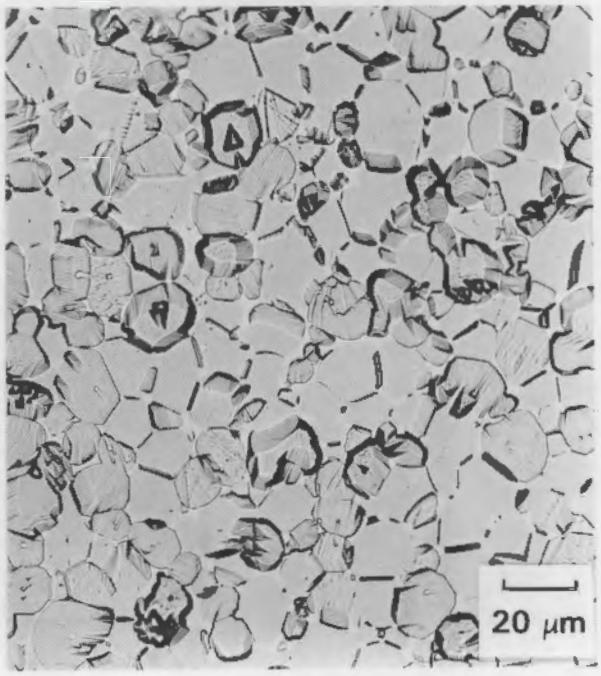


(a)

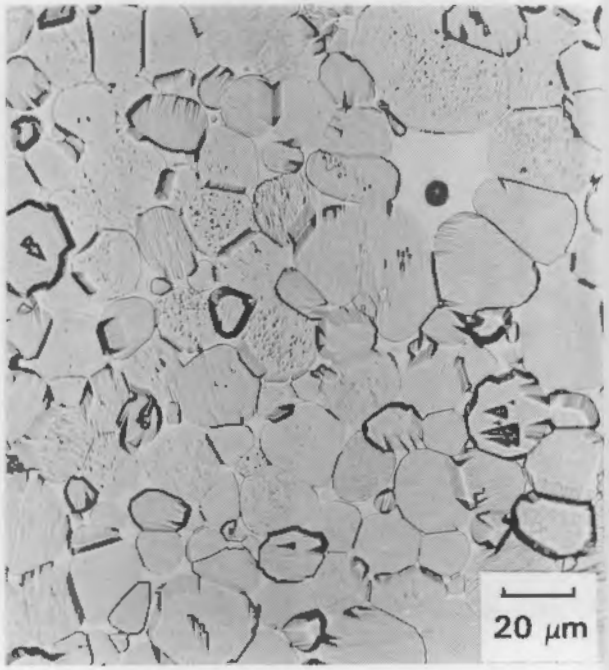


(b)

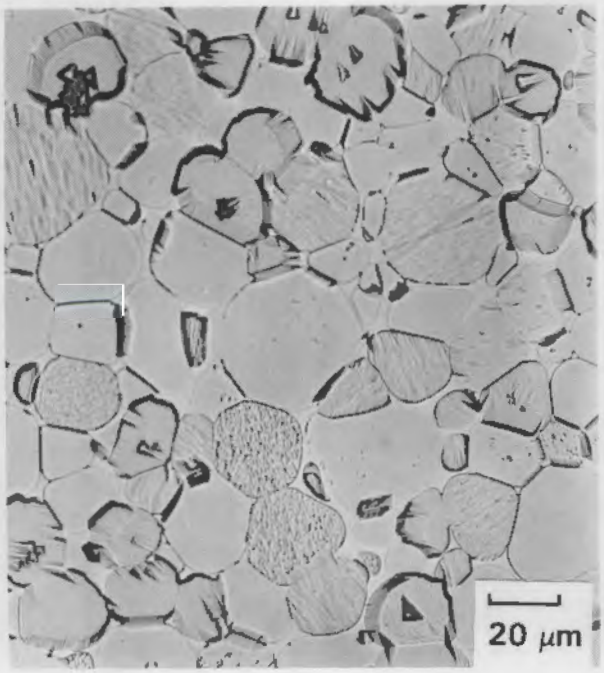


(c)

FIGURE 11. Metallographs of 97W-2.1Ni-0.9Fe Alloy Sintered at 1495°C (furnace control temperature) for (a) 4, (b) 8, and (c) 16 min

## SINTERED 70%, 90%, AND 97% W ALLOY BARS

Small bars were isostatically pressed and sintered, with five different sintering cycles, and then turned into tensile bars. All the tensile specimens and all but one LP sintered 70% W specimen failed brittlely before the yield point; high S contents found in the fracture surfaces were the likely source of embrittlement, which might be avoided by more thorough calcination or absolutely avoided by the use of nitrate (rather than sulfate) salts of Ni and Fe. Nevertheless, the relationships found between the sintering cycles, microstructure, and as-sintered hardness show that the SS sintered materials have some unique properties.

### PROCEDURES

Powders of the three alloys containing 70%, 90%, and 97% W (remainder Ni and Fe in the ratio 7/3) were prepared according to the procedures previously discussed. Calcination of the freeze-dried salts at 850°C for 6 h was followed by reduction in $H_2$ at 850°C for 2 h. The powders were prepared for isostatic pressing by tumbling in a Turbula® shaker with a few 0.5-in.-diameter stainless steel balls for 0.5 h. This treatment broke down the low-density powder spheroids and increased the bulk density of the powders from around 1 g/cc to ~3 g/cc. The powders were then isopressed in wet bag tooling at 26,000 psi into 48% dense rods ~0.45 in. in diameter and 3 in. long.

Substantial changes were made in the sintering furnace control in order to obtain precise sintering results for these bars. First, the mechanical controller was replaced with a microprocessor-based programmer controller. Second, the control thermocouple was extended into the center of the hot zone, directly over and within 0.5 in. of the sintering bars. Third, the thermocouple and sintering bars were shaded from the direct radiation of the heating elements by covering them with a piece of 50-mil-thick zirconia felt. Three closely spaced bars, one of each alloy, were sintered in each

---

® A trademark of Glen Mills, Inc., Maywood, New Jersey.

sintering run; the bars were placed on high purity alumina sand for SS sintering and for LP sintering they were partially buried in the sand for shape retention.

Single bars of each alloy were pressed and sintered for each of the following sintering cycles: 1) 1200°C-80 min (the lowest SS sintering temperature at which we were sure of obtaining full densification), 2) 1440°C-1 h (the highest SS sintering temperature), 3) 1440°C-4 h (the maximum amount of SS structural development), 4) 1485°C-10 min (flash LP sintering to minimize W spheroid growth), and 5) 1480°C-30 min (typical LP sintering temperature and time for the 90% W alloy).

As illustrated in Figure 12, SS sintering for the 1200°C-80 min cycle had a double reduction step, which was intended to maximize the reducing effects of hydrogen before a significant amount of sintering took place; the 1 h hold at 800°C was followed by a slow, 2°C/min rise to 900°C, during which time the reduction process sped up and some sintering probably began. The same heating ramps were used for the 1440°C-1 h and 1440°C-4 h SS sintering cycles. The LP sintered bars were first SS sintered at 1200°C for 80 min to 100% density, and then vacuum outgassed at 1000°C for 2 h followed by resetting in alumina sand and LP sintering at 1480°C for either 10 or 30 min. All sintering was done in 100% dry hydrogen. All fully sintered bars, about 0.36 in. in diameter and 2.3 in. long, were outgassed at 1000°C for 2 h; the outgassing conditions were chosen using the guidelines given by Yoon et al. (1983).

Immersion densities (ASTM B311) and hardnesses (HRA, corrected for the bar diameter and converted to HRC) were measured on the sintered and outgassed bars, which were then machined into small-size tensile specimens (0.160 in. in diameter) and then tested according to ASTM E8. All tensile specimens were given a second, precautionary outgassing at 1000°C and then their gage sections were polished in the longitudinal direction with 600-grit SiC paper before testing at a strain rate of 0.008 in./min. Extensometry was used to determine the yield point at 0.2% offset.

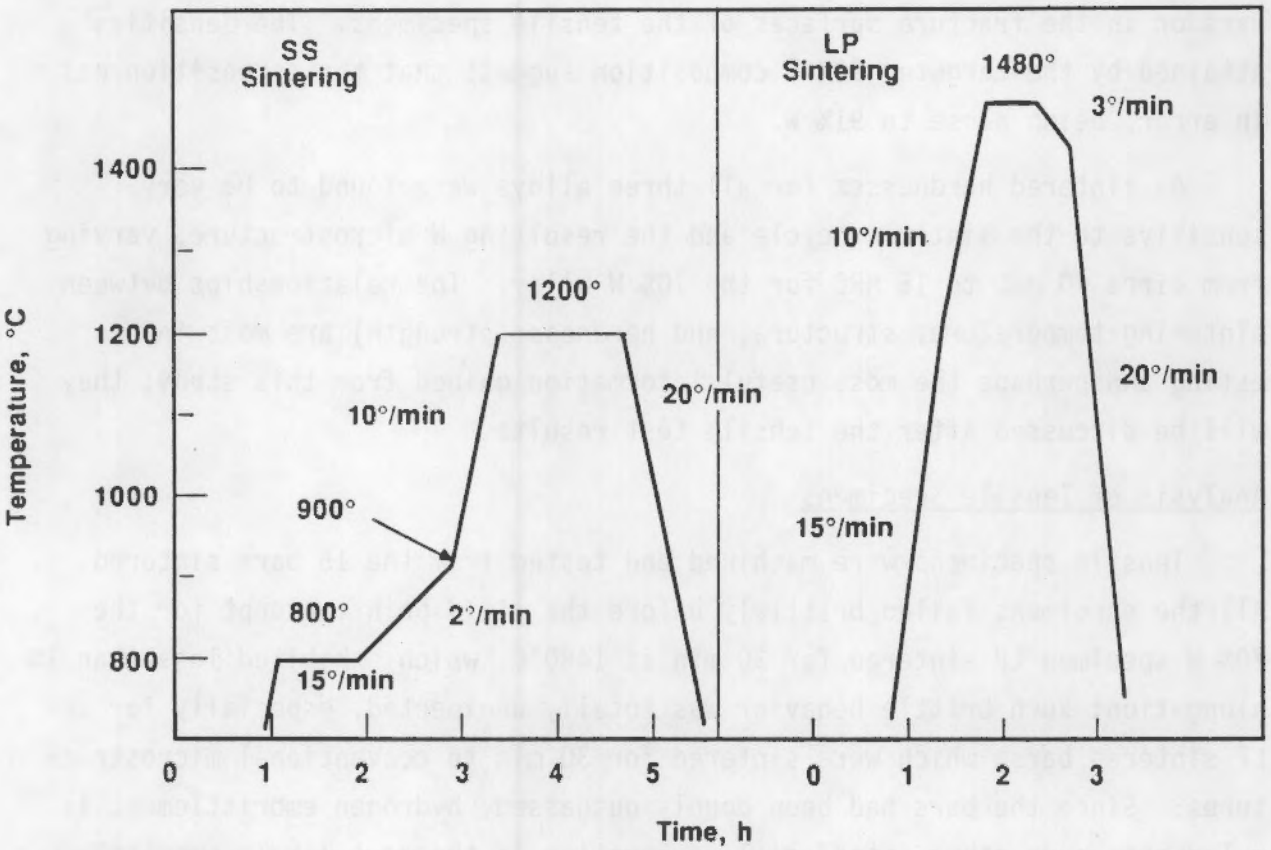


FIGURE 12. Sintering Cycles for Bars (in 100% dry hydrogen). Only the peak temperature and time were varied for alternate cycles. All sintered bars vacuum outgassed 2 h at 1000°C.

## RESULTS AND DISCUSSION

All of the bars sintered to theoretical density with little variation in density between the 5 sintering cycles:

| | |
|---|---|
| 70% W | 14.06 to 14.09 g/cc |
| 90% W | 14.33 to 14.39 g/cc |
| 97% W | 18.52 to 18.54 g/cc |

There was no blistering observed either on the surfaces of the as-sintered bars or in the fracture surfaces of the tensile specimens. The densities attained by the targeted 90% W composition suggest that the composition was in error, being close to 91% W.

As-sintered hardnesses for all three alloys were found to be very sensitive to the sintering cycle and the resulting W microstructure, varying from circa 40 HRC to 15 HRC for the 70% W alloy. The relationships between sintering temperature, structure, and hardness (strength) are most interesting and perhaps the most useful information gained from this study; they will be discussed after the tensile test results.

Analysis of Tensile Specimens

Tensile specimens were machined and tested from the 15 bars sintered. All the specimens failed brittlely before the yield point, except for the 70% W specimen LP sintered for 30 min at 1480°C, which exhibited less than 1% elongation; such brittle behavior was totally unexpected, especially for the LP sintered bars, which were sintered for 30 min to conventional microstructures. Since the bars had been doubly outgassed, hydrogen embrittlement is ruled out; some other interfacial segregation is the most likely embrittlement source (Gurwell 1986). Therefore, a single 90% W specimen which had been LP sintered at 1480°C for 10 min was fractured and examined by high-resolution Auger electron spectroscopy (AES). Also, selected chemical analyses for typical interfacial segregants were performed on all three compositions sintered at 1480°C for 10 min. Selection of a 90% W LP sintered specimen allowed direct comparisons to be made with a highly ductile (30% elongation), similar structure, LP sintered 90% W specimen made from conventional powders.

Analysis of the interfacial chemistries was done with a scanning Auger electron spectrometer, which has a spatial resolution of 300 Å. The sample was fractured in situ in the AES chamber. Analysis of the fracture surface was performed with a 10 keV, 200 nanoampere beam; data was taken in the N(E) pulse count mode and differentiated for analysis. Four regions of the fracture were examined and in each region the three types of interfaces shown in Figure 13 were analyzed: 1) the W-W contact area, 2) the W surface of a

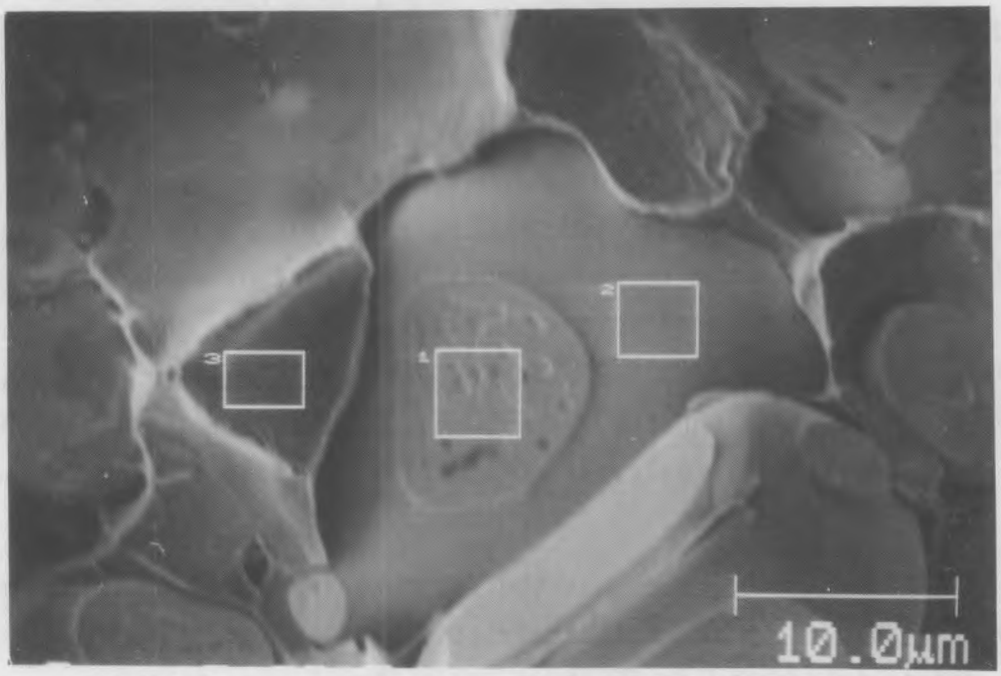


FIGURE 13. Scanning Electron Micrograph Showing Typical Areas Analyzed by Auger Electron Spectroscopy. 90% W, LP sintered 10 min at 1480°C. 1) W-W interface, 2) W-matrix interface (W side), 3) matrix-W interface (matrix side).

W-matrix interface, and 3) the matrix side of the W-matrix interface. There is a complete lack of W cleavage in the fracture surfaces, which is characteristic of brittle heavy alloys with heavy interfacial segregation.

Analyses of each interface type were consistent for all four regions examined. The average analyses obtained from all four regions are presented in Table 1. The analytical data given in Table 1 are also consistent with

TABLE 1. Elemental Concentrations at Interfaces

| | Element, at.% | | | | | | | |
|---|---|---|---|---|---|---|---|---|
| Interface | W | Ni | Fe | O | C | S | P | Si |
| W-W | 55 | 11 | 9 | 3 | 4 | 18 | <0.04 | 0.1 |
| W-Matrix | 53 | 12 | 10 | 2 | 9 | 13 | <0.04 | 0.2 |
| Matrix-W | 8 | 43 | 32 | 4 | 5 | 8 | <0.04 | 0.5 |

Elements not detected: P (<0.04), Ca (<0.05), Al (<0.14).

analyses performed previously, using the same Auger spectroscope, on high-ductility (30% elongation), LP sintered 90% W alloy (from conventional powders), except that high levels of S were found in all the interfaces of the sample derived from freeze-dried powder. The high S contents at all the interfaces are the single distinguishing features of the fracture surfaces of the sintered bars from freeze-dried powder. Sulfur segregation of greater than 0.2 monolayer is known to cause embrittlement of Ni (Bruemmer et al. 1983). The bulk S content of this sample was measured by combustion analysis (Leco Inc.) to be 15 ppm (Table 2), an unusually high level, and certainly high enough to result in enhanced interfacial S segregation. Therefore, high residual S contents are largely, if not totally, responsible for embrittlement of the LP sintered bars.

It is interesting to note that the fracture surfaces contained no detectable P (<0.04 at.% for this analysis). The addition of P to Ni is known to reduce intergranular fracture and to improve ductility because P strongly segregates to grain interfaces and limits S enrichment at the interfaces (Bruemmer et al. 1983). Perhaps small, controlled additions of P

TABLE 2. Bulk Chemical Analyses of Bars LP Sintered 10 min at 1480°C

| | Element, ppm | | | |
|---|---|---|---|---|
| W Content | O | C | S | H |
| 70 | 66 | 10 | 88 | 0.40 |
| 90 | 67 | 6 | 15 | 0.27 |
| 97 | 60 | 9 | 10 | 0.27 |
| Approximate thresholds for embrittlement[a] | | | | |
| | 20-25 | 50-100 | 15 | 0.5-1.0 |

(a) Personal communications between W. E. Gurwell and T. W. Penrice, Teledyne Firth Sterling, LaVergne, Tennessee, 1988; and W. E. Gurwell and J. A. Mullendore, GTE Products Corp., Towanda, Pennsylvania, 1988.

would have been effective in reducing or eliminating the S-induced embrittlement found in this study. However, it would appear to be safer (at least, more straightforward) to reduce the S to harmless levels, with or without P present.

The bulk chemical analyses shown in Table 2 are compared with the "threshold for embrittlement" for each element. The thresholds given are based on general experience with the normal range of 90 to 97% W alloys; since the elements in question are more soluble in the matrix than the W phase, the actual embrittling level is dependent on the amount of matrix, as well as the degree of segregation of the elements to the W-matrix interface. Nevertheless, the threshold levels given in Table 2 can be used as a guide.

The threshold for S indicates that the residual S is indeed high enough to possibly cause embrittlement. By the same token, O levels for all three alloys appear to be far in excess of the embrittlement threshold. On the other hand, the O levels in the fracture surfaces, as determined by AES, are similar to those found in high-ductility 90% W made from conventional powders. Due to the high surface area of freeze-dried powders, high O contents are expected in the powders and particular attention must be paid to the reduction of O content during sintering. Therefore, further work needs to be done to evaluate the reduction phase of the sintering cycle and to assure that O contents are reduced sufficiently. The very high surface area of the powders may be an impediment to attaining suitably low O content during sintering, at least for the 0.4-inch-diameter bars sintered in this study; thicker powder pressings will be harder to reduce. The reduction process is controlled by diffusion of $H_2$ into the part and water vapor out of the part; the time required to adequately reduce the O content will be proportional to the square of the part thickness. Also, it is important to remember that diffusion rates are slower for the high surface area powders derived from freeze drying (relative to conventional powders) and that the O content of freeze-dried powders is higher in keeping with the high surface area.

The bulk C contents given in Table 2 for the sintered bars are too low to cause embrittlement; also, the C concentrations at the fracture surface,

as determined by AES, are slightly lower than those found in high-ductility 90% W from conventional powders. The measured $H_2$ contents are also below the embrittlement level, although lower $H_2$ levels, less than 0.05 ppm, have been measured on 90% W (from conventional powders), which was singly outgassed under identical conditions. If the $H_2$ analyses are assumed to be correct, then there may be an impurity present in the material that is trapping or holding $H_2$.

Sintering Temperature, Structure, and Hardness Relationships

Table 3 contains the as-sintered densities and hardnesses for all 15 bars sintered. The densities for each alloy are very consistent despite the wide variation in sintering conditions, indicating that full densification was consistently achieved.

TABLE 3. Properties of Sintered Bars

| Sinter Cycle | Density, g/cc | Hardness, HRC | Estimated W Particle Size, μm | |
|---|---|---|---|---|
| | | | Range | Midrange |
| 70% W (44 vol% W phase) | | | | |
| 1200°C-80 min | 14.06 | 39 | 1-2 | 1.5 |
| 1440°C-1 h | 14.07 | 24 | 3-6 | 4.5 |
| 1440°C-4 h | 14.07 | 20 | 4-7 | 5.5 |
| 1485°C-10 min | 14.09 | 15 | 7-15 | 11 |
| 1480°C-30 min | 14.07 | 15 | 10-20 | 15 |
| 90% W (79 vol% W phase) | | | | |
| 1200°C-80 min | 17.39 | 42 | 2-4 | 3 |
| 1440°C-1 h | 17.33 | 25 | 5-9 | 7 |
| 1440°C-4 h | 17.34 | 27 | 5-10 | 7.5 |
| 1485°C-10 min | 17.35 | 22 | 12-25 | 18.5 |
| 1480°C-30 min | 17.35 | 19 | 15-30 | 22.5 |
| 97% W (93 vol% W phase) | | | | |
| 1200°C-80 min | 18.53 | 43 | 4-8 | 6 |
| 1440°C-1 h | 18.53 | 28 | 8-16 | 12 |
| 1440°C-4 h | 18.52 | 26 | 10-20 | 15 |
| 1485°C-10 min | 18.54 | 25 | 17-30 | 23.5 |
| 1480°C-30 min | 18.54 | 28 | 20-30 | 25 |

Hardnesses of the alloys were unusually high for the 1200°C sinter; the hardness of the 70% W alloy sintered at 1200°C is remarkably high with respect to the low W-phase content in the alloy, 44 vol%. In fact, the 70% W alloy hardness is nearly equal to the hardnesses of the 90% and 97% W alloys. The hardnesses decreased with increasing sintering temperature, as shown in Figure 14, due to coarsening of the structure (grain growth) illustrated in Figure 15. The W particle sizes listed in Table 3, and plotted as a function of sintering temperature in Figure 15, were visually estimated from fractographs of the individual tensile bars, Figures 16 through 20. (Please

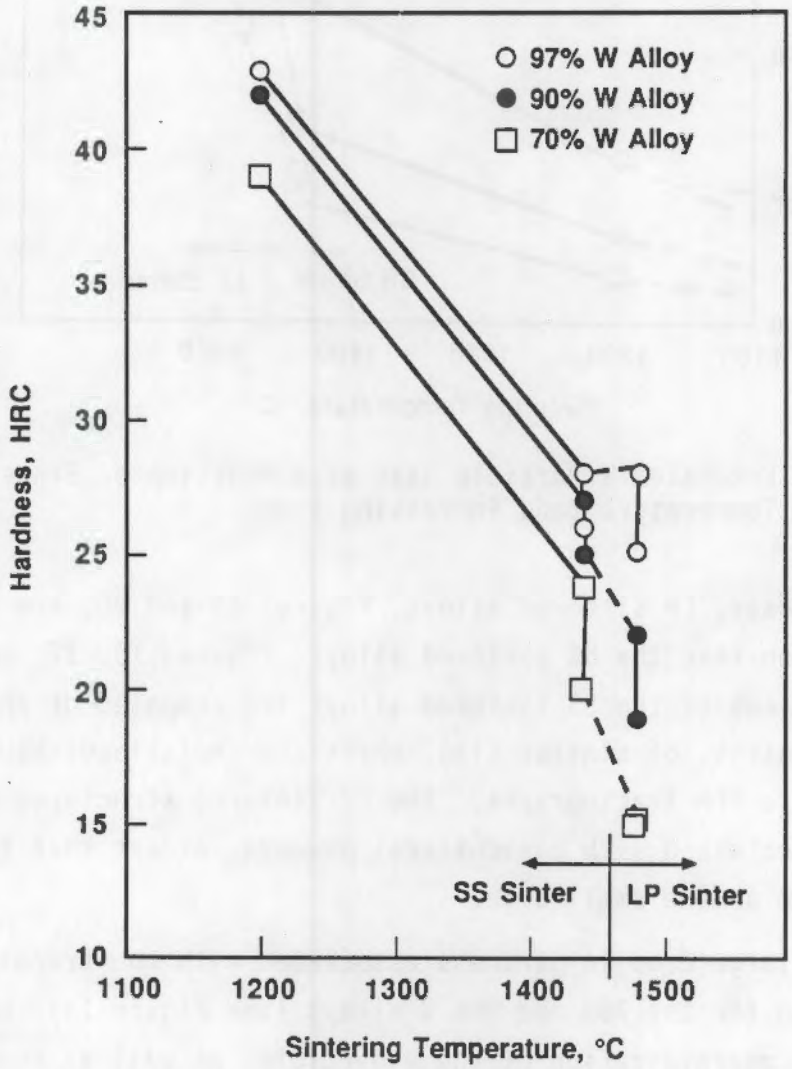


FIGURE 14. Hardness of Sintered Bars as a Function of Sintering Temperature (and increasing time)

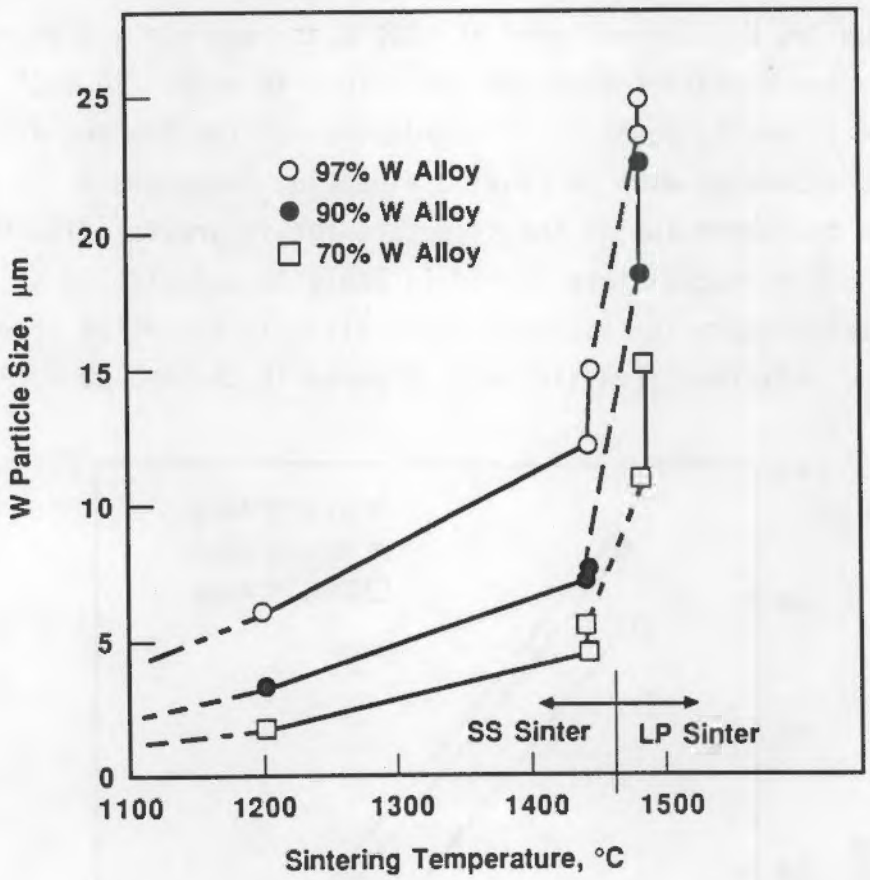


FIGURE 15. Estimated W Particle Size as a Function of Sintering Temperature (and increasing time)

note that the coarser, LP sintered alloys, Figures 19 and 20, are shown at a lower magnification than the SS sintered alloys, Figures 16, 17, and 18.) The fracture surfaces of the SS sintered alloys are composed of polygonal grains of W and matrix, of similar size, which are indistinguishable from each other in these SEM fractographs. The LP sintered structures are very typical of those obtained with conventional powders, except that the W particle sizes are on the small side.

There was a large drop in hardness associated with the transition from SS to LP sintering for the 70% and 90% W alloys (see Figure 14), which may be due, in part, to spheroidization of the W particles as well as coarsening of the structure. The 97% W alloy exhibited little hardness change during the transition from LP to SS sintering because 1) there was somewhat less

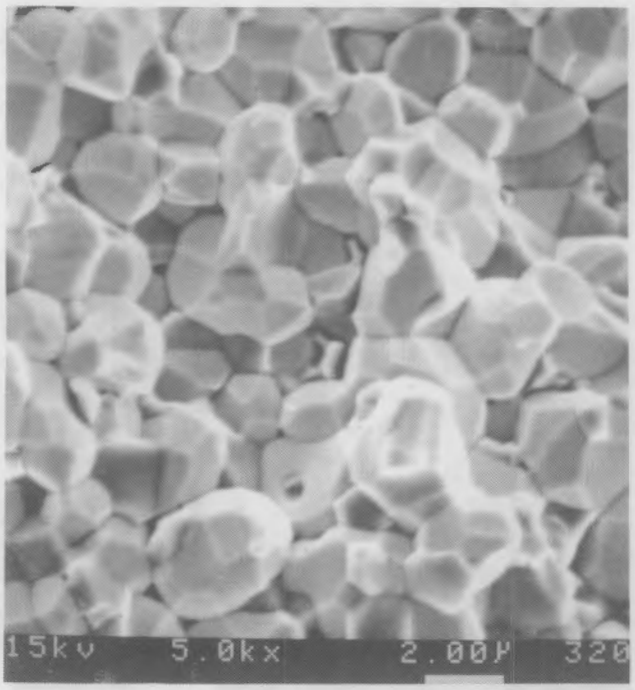


90% W

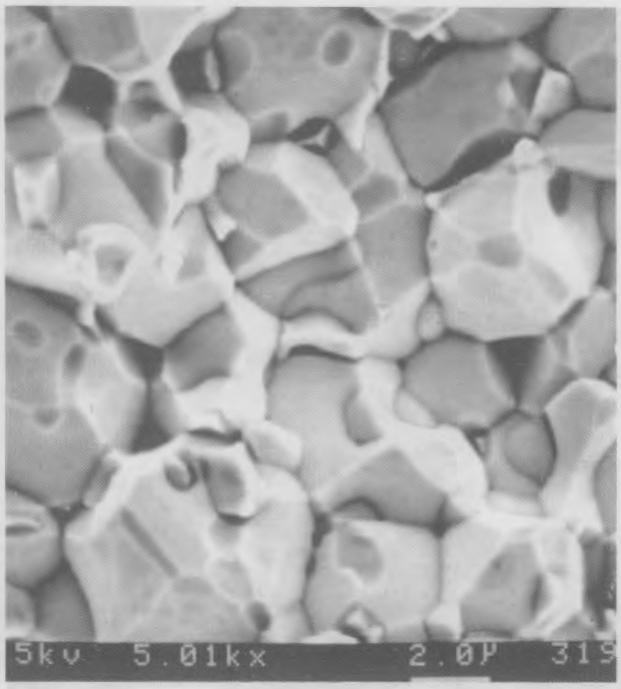


97% W

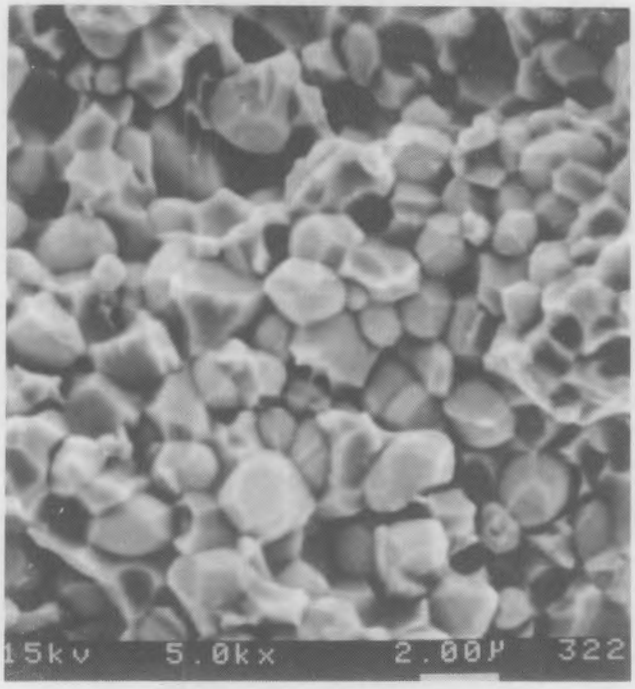


70% W

FIGURE 16. Scanning Electron Fractographs of Bars SS Sintered at 1200°C for 80 min

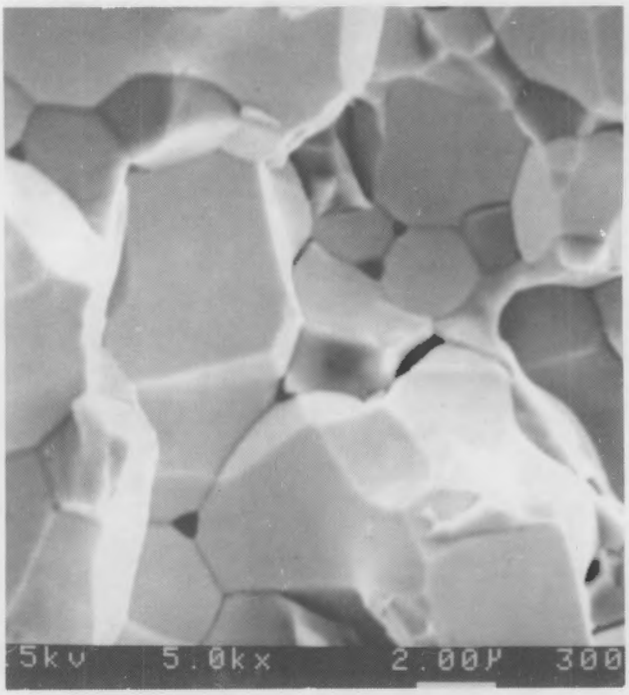


90% W

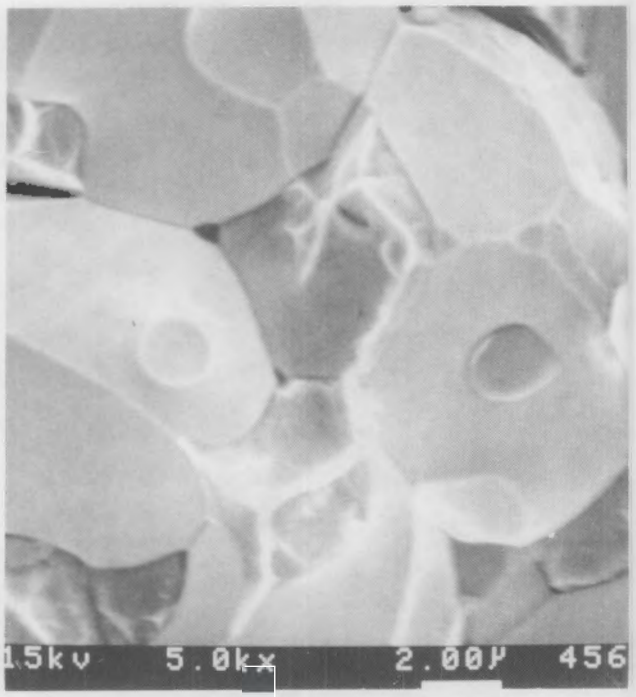


97% W

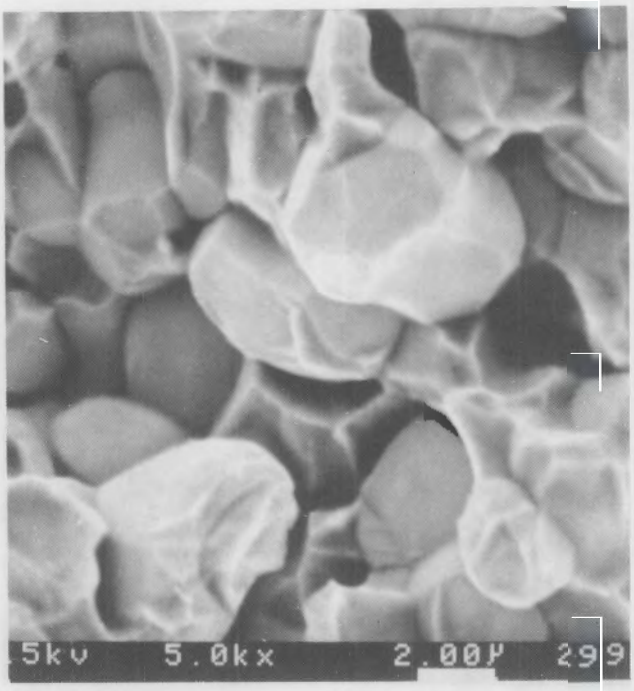


70% W

FIGURE 17. Scanning Electron Fractographs of Bars SS Sintered at 1440°C for 1 h

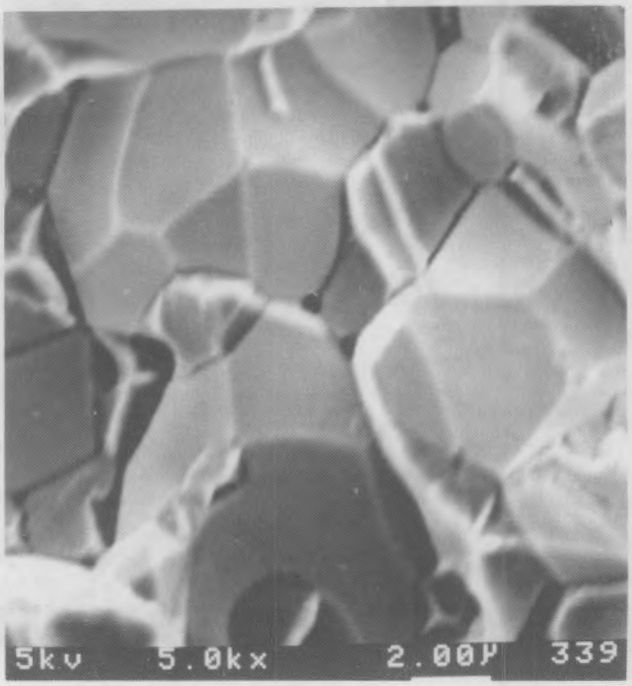


90% W

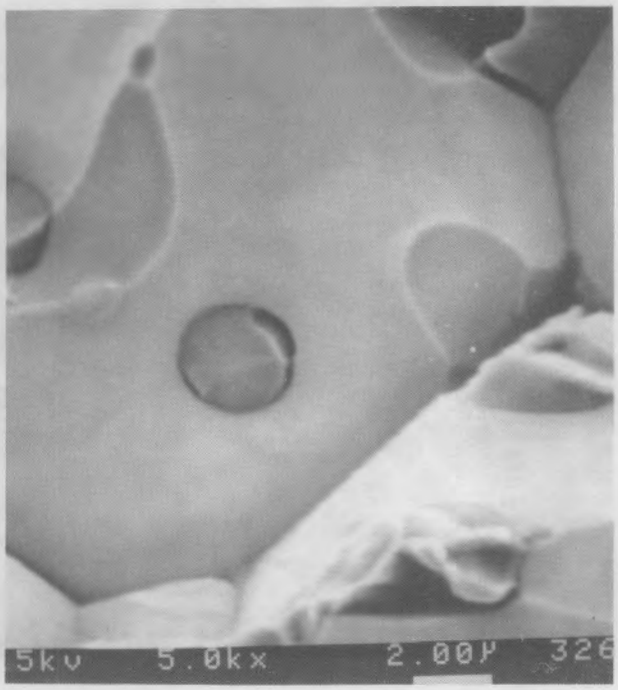


97% W

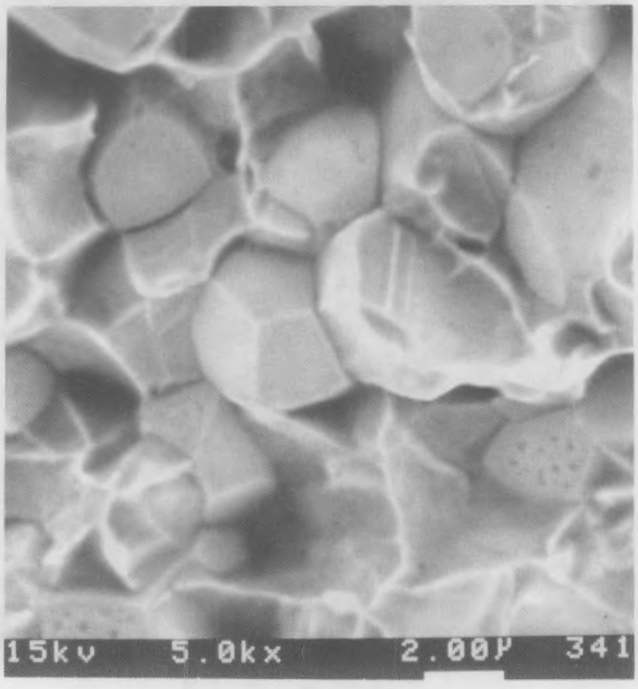


70% W

FIGURE 18. Scanning Electron Fractographs of Bars SS Sintered at 1440°C for 4 h

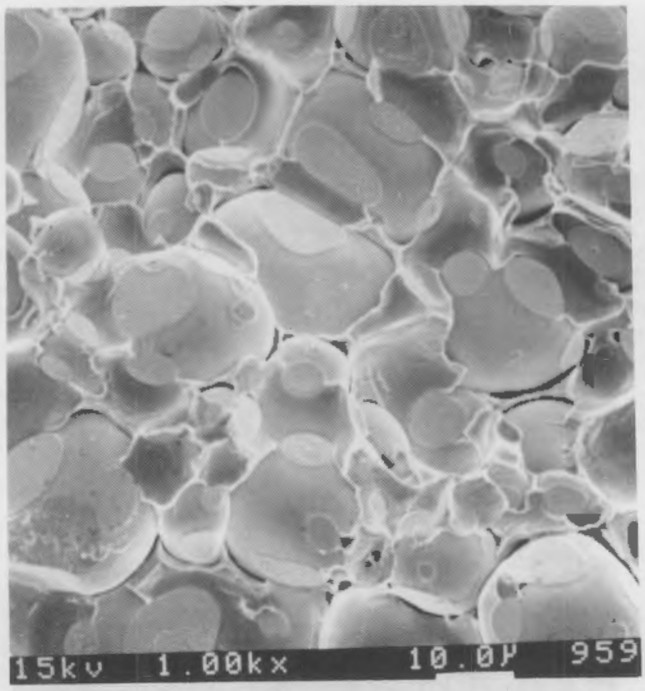


90% W

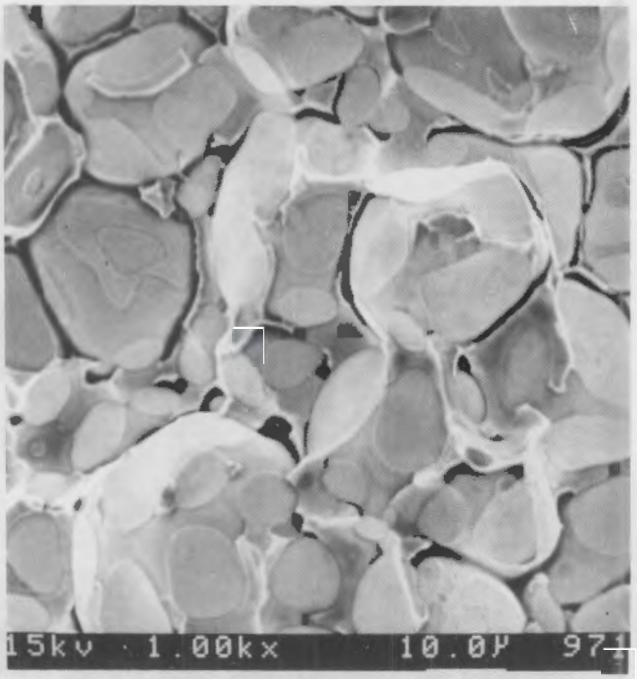


97% W

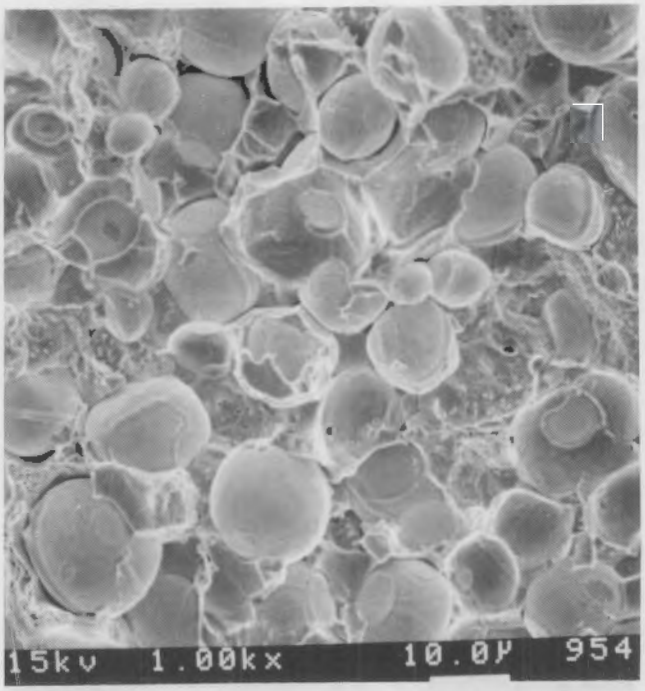


70% W

FIGURE 19. Scanning Electron Fractographs of Bars LP Sintered at 1485°C for 10 min

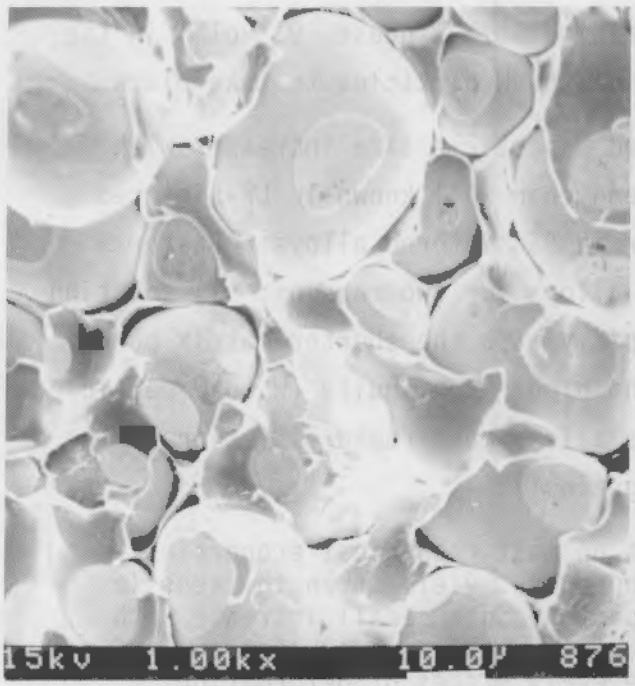


90% W

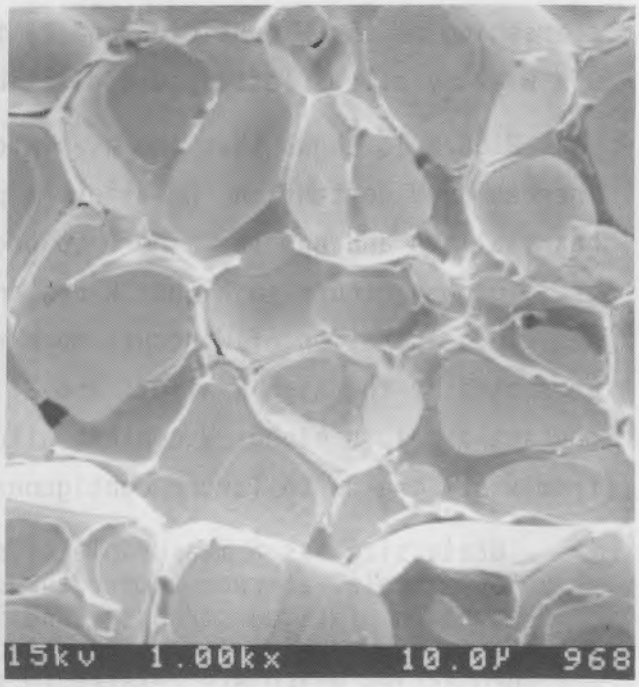


97% W

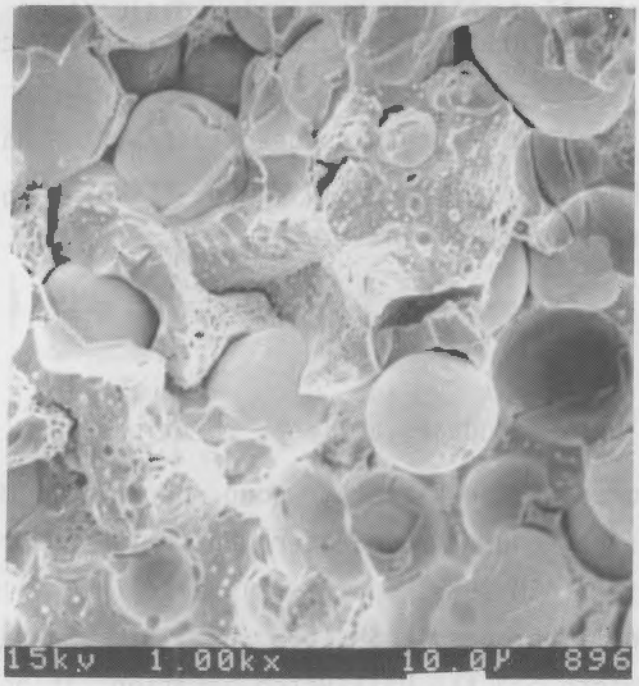


70% W

FIGURE 20. Scanning Electron Fractographs of Bars LP Sintered at 1480°C for 30 min

coarsening of the W particles and 2) the high vol% W phase (93 vol%) in the 97% W alloy allows less spheroidization of the W particles to take place.

Figure 15 shows that the as-sintered W particle size increases with increasing W content in the alloy, a phenomenon well known in LP sintered heavy alloys and now shown here to occur in SS sintered alloys. Faster W grain growth occurs in higher W content alloys for two reasons: 1) solution and reprecipitation of W occurs more rapidly with the shorter matrix path presented by the high W alloy, and 2) the higher contiguity (W-to-W particle contact area) in higher W content alloys allows more rapid diffusion of the W from small grains to larger contiguous grains.

> "Grain size has a measurable effect on most mechanical properties. For example, at room temperature, hardness, yield strength, tensile strength, fatigue strength, and impact resistance all increase with decreasing grain size. The effect of grain size is largest on properties which are related to the early stages of deformation, for it is at this stage that grain-boundary barriers are most effective. Thus, yield stress is more dependent on grain size than tensile strength. For the latter stages of deformation the strength is controlled chiefly by complex dislocation interactions occurring within the grains, and grain size is not a controlling variable." (Dieter 1961, p. 121).

The effect of grain size on strength is described by the Hall-Petch relationship (Dieter 1961, pp. 121, 189, 205) in which strength, $c_o$, is inversely related to the square root of grain size:

$$c_o = c_i + K_y D^{-1/2}$$

A plot of $c_o$ versus $D^{-1/2}$ produces a linear relationship.

Hardness, measured by the Vickers, Knoop, or Brinell methods, is equal to the average pressure under the indenter, which is proportional to the flow stress of the material (ASM 1985, pp. 71-72); also, HRC is nearly proportional to Brinell hardness (ASM 1985, p. 110). Therefore, HRC is proportional to strength and the Hall-Petch equation can be used to model the relationship between hardness, HRC, and grain size.

The hardness data from Table 3 are plotted on a Hall-Petch diagram, Figure 21. Linear regression was used to fit the data for each alloy to a

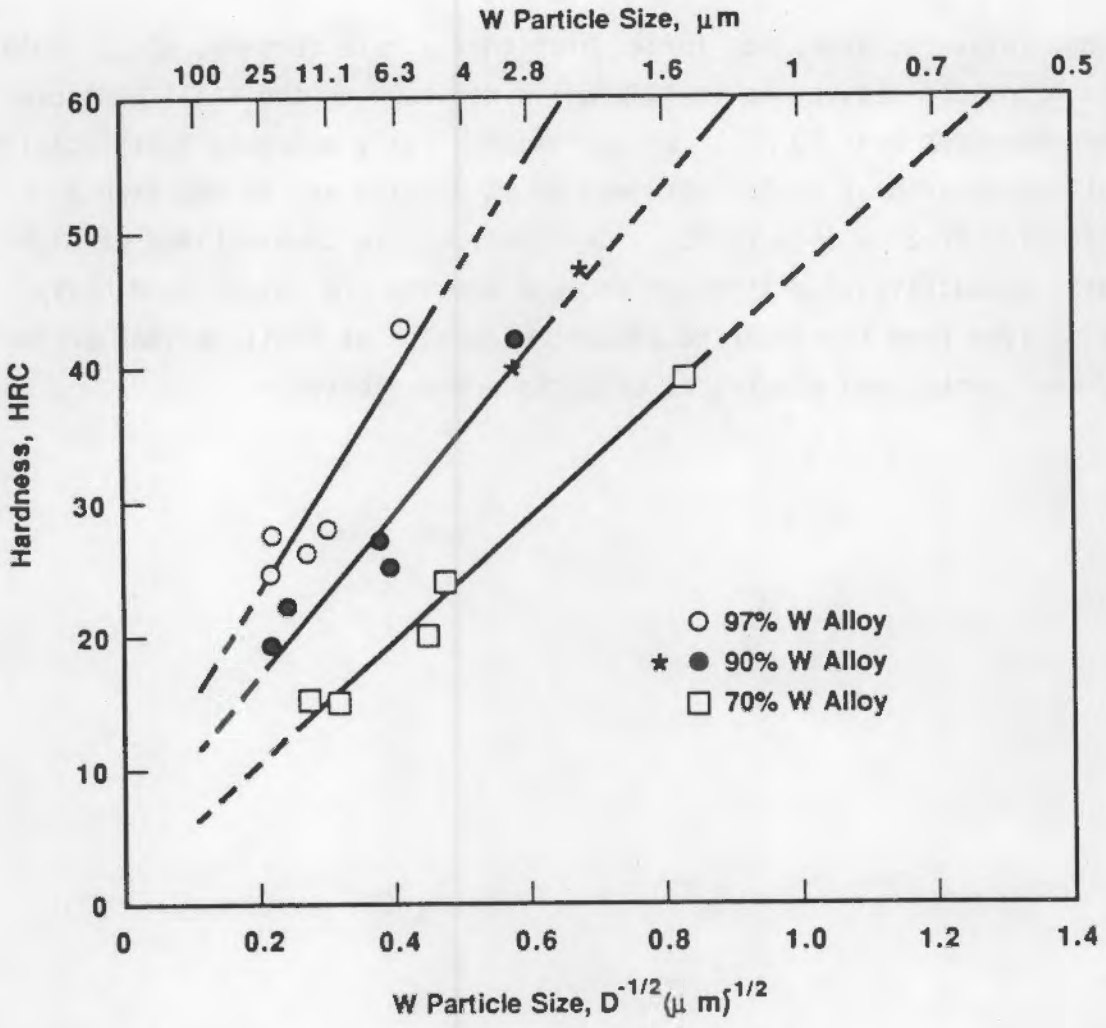


FIGURE 21. Hall-Petch Diagram of Hardness Versus Estimated W Particle Size. All data points from Table 3 except asterisks (*), which are from Figure 22.

straight line. Extrapolation of the straight lines to finer particle sizes (from lower sintering temperatures) indicates that hardnesses as high as 60 HRC are possible for all three alloys, if the sintering temperature could be lowered sufficiently. For example, Figure 21 indicates that the 90% W alloy would be 60 HRC at a particle size of approximately 1.2 μm. Loosely extrapolating the curve for the 90% W alloy in Figure 15, a 1.2-μm W particle size is obtained at a processing temperature of 1000°C to 1050°C. Figure 22 contains a micrograph of a 90% W button sintered 2 h at 1030°C. The W particle size is about 1 μm, as predicted, but the material is only 92.5% dense with 48 HRC; further low temperature processing by hot isostatic

pressing, forge-resinter, hot forge, high-energy rate forming, etc., could be used to bring the density up to 100% while maintaining the small particle size and hardness near 60 HRC. Without mechanically enhanced densification, the button sintered at 1130°C attained 99.9% density and 48 HRC with a particle size of 2 μm (Figure 22). Certainly, these combinations of high hardness, conductivity, melting point, and density are unique to W heavy alloys derived from freeze-dried powder; uses such as small caliber projectiles, wear parts, and electrical contacts are suggested.

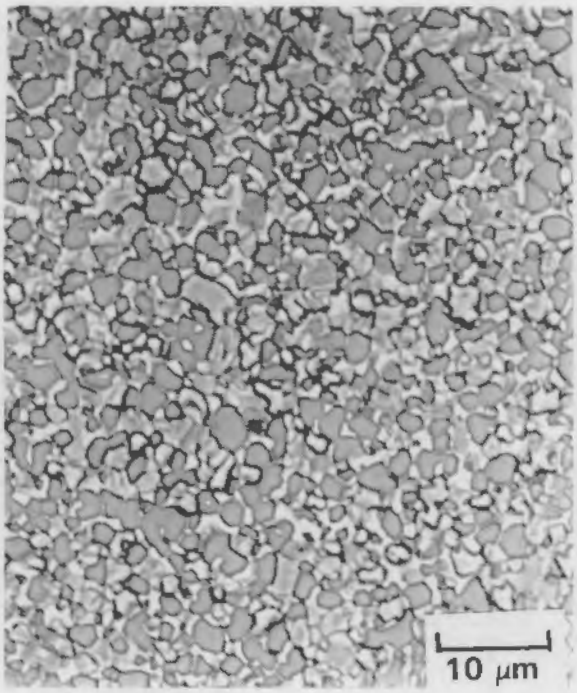


1130°C-99.9% Dense
48 HRC W Particle ~2 μm

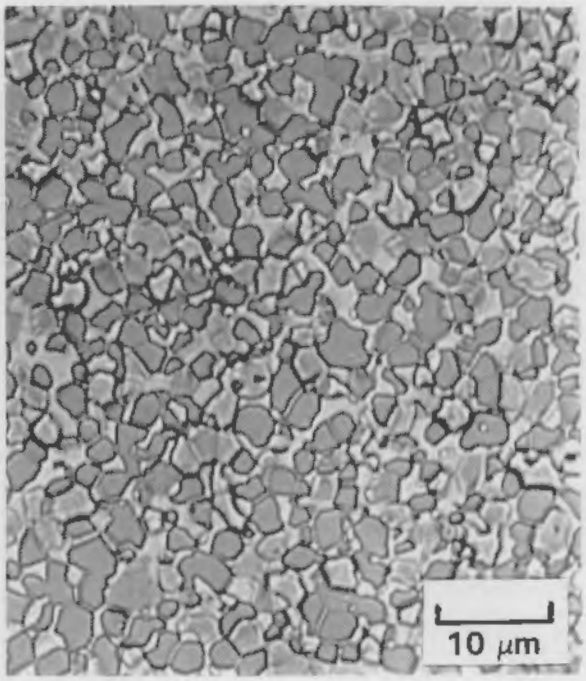


1240°C-100% Dense
41 HRC W Particle ~3 μm

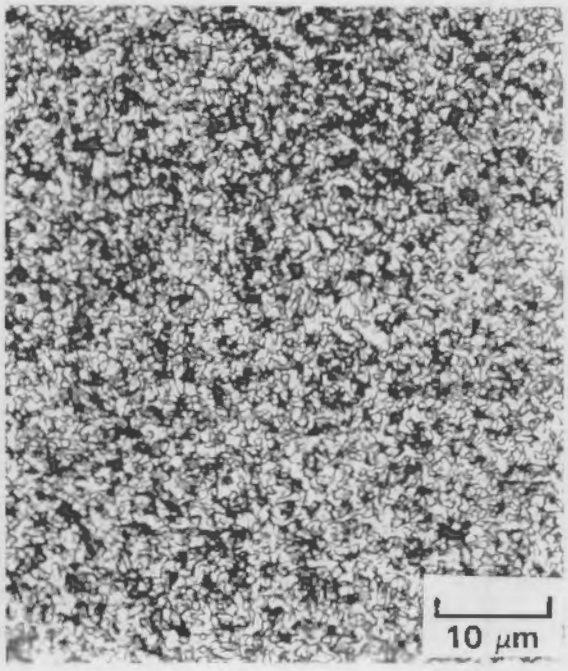


1030°C-92.5% Dense
48 HRC W Particle ~1 μm

FIGURE 22. Development of Microstructure, Density, and Hardness in 90% W Alloy by SS Sintering for 2 h at 1030°C, 1130°C, and 1240°C. Hardness and W particle sizes obtained at 1130°C and 1240°C agree with the Hall-Petch plot (Figure 21) of the data in Table 3. The low density at 1030°C drops the hardness considerably, from 60 HRC, theoretically, at 100% density to 48 HRC.

## REFERENCES

American Society for Metals (ASM). 1985. Mechanical Testing, Volume 8 of Metals Handbook, 9th ed. ASM International, Metals Park, Ohio.

Bruemmer, S. M., R. H. Jones, M. T. Thomas, and D. R. Baer. 1983. "Influence of Sulfur, Phosphorus, and Antimony Segregation on the Intergranular Hydrogen Embrittlement of Nickel." Metall. Trans. A 14A(2):223-232.

Dieter, G. E. 1961. Mechanical Metallurgy. McGraw-Hill, New York.

Gurwell, W. E. 1986. "A Review of Embrittlement Mechanisms in Tungsten Heavy Alloys." In Progress in Powder Metallurgy, Volume 42. Metal Powder Industries Federation, Princeton, New Jersey.

Landsberg, A. 1967. "Preparation of Homogeneous Powders Composed of Ultrafine Particles." U.S. Patent 3,357,819.

Landsberg, A., and T. T. Campbell. 1965. "Freeze-Dry Technique for Making Ultrafine Metal Powder." J. Metals 17:846-860.

Roehrig, F. K., and T. R. Wright. 1972. "Freeze Drying: A Unique Approach to the Synthesis of Ultrafine Powders." J. Vac. Sci. Technol. 9(6):1368-1372.

Schnettler, F. J., F. R. Monforte, and W. W. Rhodes. 1968. "A Cryochemical Method for Preparing Ceramic Materials." In Science of Ceramics, Volume 4, pp. 79-90. The British Ceramic Society, Stoke-on-Trent, England.

Yoon, H. K., S. H. Lee, S.-J. L. Kang, and D. N. Yoon. 1983. "Effect of Vacuum-Treatment on Mechanical Properties of W-Ni-Fe Heavy Alloy." J. Mater. Sci. 18:1374-1380.

# DISTRIBUTION

No. of Copies

OFFSITE

10 Office of Scientific and Technical Information

5 Director
U.S. Ballistic Research Laboratory
Aberdeen Proving Ground, MD 21005-5066
ATTN: W. J. Bruchey/SLCBR-TB-A
R. Coates/SLCBR-TB-P
E. Horwath/SLCBR-TB-A
E. Kennedy/SLCBR-TB-P
L. Magness/SLCBR-TB-P

U. S. Army Materials Testing Laboratory
Arsenal Street
Watertown, MA 02172
ATTN: K. H. Tauer (Bldg 3135)

2 Battelle Columbus Laboratory
505 King Ave.
Columbus, OH 43201-2693
ATTN: H. B. Cialone
R. Fiorentino

3 Teledyne Firth Sterling
#1 Teledyne Place
LaVergne, TN 37086
ATTN: S. G. Caldwell
T. W. Penrice
J. Bost

Climax Specialty Metals
21801 Tungsten Road
Cleveland, OH 44117
ATTN: J. P. Linteau

2 CarTech
101 West Bern Street
P.O. Box 14662
Reading, PA 19612-4662
ATTN: G. J. Del Corso
D. Esposito

No. of Copies

Ametek, Inc.
21 Toelles Road
Wallingford, CN 06492
ATTN: A. Juraska

2 GTE Sylvania
Hawes Street
Towanda, PA 18848
ATTN: J. A. Mullendore
J. R. Spencer

3 Kennametal, Inc.
Latrobe, PA 15650
ATTN: H. O. Patricia
D. Boy
W. F. Copeland

ONSITE

DOE Richland Operations Office

J. J. Sutey, A5-90

32 Pacific Northwest Laboratory

E. L. Courtright, K3-59
G. B. Dudder, P8-33
W. E. Gurwell, P8-35 (20)
R. S. Kemper, K2-22
K. A. Parnell, P7-18
K. R. Sump, P8-35
G. D. White, P8-35
Technical Report Files (5)
Publishing Coordination